ARTICLE TYPE

# Distributed event-triggered fixed-time formation tracking control for multi-spacecraft systems based on adaptive immersion and invariance technique

Xia Wu[1] | Caisheng Wei*[2]

[1]School of Electronic Information, Hunan First Normal University, Changsha, Hunan, 410205, China

[2]School of Automation, Central South University, Changsha, Hunan, 410083, China

**Correspondence**
*Caisheng Wei, Central South University.
Email: caisheng_wei@csu.edu.cn

**Abstract**

The problem of fixed-time formation tracking for multi-spacecraft systems without internal collisions is investigated in this paper. A novel adaptive immersion and invariance (I&I)-based control protocol is designed to solve this technical problem, with the goal of driving formation members to accurately realize and maintain the required configuration within the user-given time. The novelty here lies in two things. First and foremost, unlike the asymptotic convergence of the traditional I&I related works, the proposed protocol guarantees the fixed-time stability by integrating the prescribed performance control. Secondly, the event-triggered mechanism is adopted to alleviate the pressure of communication resources between formation members and reduce unnecessary information interaction. Lyapunov stability analysis shows that the proposed protocol can enable the defined implicit manifold to converge to the origin for most initial conditions. Also, benefiting from the prescribed performance techniques, the convergence time eliminates the dependence of designed controller parameters or initial system conditions, relying only on the actual mission requirements. In addition, we adopt a linear extended state observer to deal with the parameter uncertainties and external disturbances, and use the I&I adaption to estimate the observer errors to further improve the system performance. Moreover, a new exponential-type artificial potential function is designed to avoid close proximity between formation members and prevent internal collisions. Finally, numerical simulations are provided to verify the theoretical results.

**KEYWORDS:**
Formation tracking for multi-spacecraft systems; Adaptive immersion and invariance-based control protocol; Event-triggered mechanism; Exponential-type artificial potential function; Required formation configuration

## 1 | INTRODUCTION

The concept of multi-spacecraft formation was put forward by Sholomitsky et al. in 1977 when conducting infrared synthetic aperture imaging of multiple spacecraft[1]. Spacecraft formation flying (SFF) is a way to spread the functions of a large spacecraft over numerous smaller ones, which can improve system reliability, robustness, and launch flexibility while reducing costs[2].

---

[0]**Abbreviations:** LVLH, local vertical local horizontal; ECI, Earth center inertial

These advantages make SFF receive extensive attention, and has been widely used in complicated space missions[3,4,5]. Generally, SFF technique contains formation reconstruction and formation maintenance. Formation reconstruction is needed to adapt to the expected configuration changes caused by different mission requirements. Formation maintenance requires that the nominal configuration can be accurately maintained even in the presence of space disturbance[6]. While SFF is evolving, there are still significant technical challenges in the area of control design for formation reconfiguration and maintenance. Parametric uncertainties, mission timeliness, formation accuracy, communication resource pressure and possible internal collisions are all problems faced by SFF research. Nevertheless, the search for SFF control is still in full swing and has yielded fruitful results[6,7,8,9].

Adaptive control is a useful tool for uncertain systems with unknown or slow time-varying parameters. Since emerging in the 1950s, it has been extensively studied in various practical situations such as flight control and robotic systems, especially in recent decades[10,11]. Lyapunov synthesis method is one of the most well-known techniques in adaptive control, which requires to construct a Lyapunov function. But at present, the choice of the Lyapunov function still depends on experience accumulation and trial-and-error, lack of systematic methods. This becomes even more difficult when faced with complex nonlinear systems. Furthermore, due to its inherent nonlinearity, adaptive control is very sensitive to model uncertainties and external disturbances, which may lead to system performance degradation or even instability. This greatly limits its scope of application[12]. Many efforts have been made to bridge this gap. Among them, one representative result is the adaptive immersion and invariance (I&I) control, which is a model reduction method that does not require the theory of a Lyapunov function, thus circumventing the problem of Lyapunov function selection in the adaptive law design of conventional adaptive control[13]. Adaptive I&I control is the inheritance and development of I&I technology. The essence of I&I theory is to select an appropriate immersion mapping and a target system with desired behavior, so that the states of the controlled system are the images of the target system under the selected mapping, and then design a control law to transform the image into an invariant attractive manifold to ensure the stability of the controlled system. Obviously, the proper selection of the target system plays an important part in obtaining the mapping. I&I theory has been widely used since it was designed by Astolfi et al. in 2003, i.e., flight control systems, electromechanical system, mobile Robots and so on[14,15,16,17]. As a derivative of the I&I theory, the adaptive I&I control has a notable innovation compared with other adaptive control techniques is the addition of an auxiliary regulation term $\beta$ to the adaptive law, which not only reduces the parameter estimation error, but also facilitates the subsequent stability analysis[12]. Naturally, the adaptive I&I control has also been widely sought after since it was proposed, and has obtained many successful applications. Related works can be found in 18,19,20,21 and references therein. Recently, I&I related techniques have also been applied to the cooperative control of the multi-agent systems, and many interesting results have been derived[22,23].

Notably, the aforementioned related works are continuous-time-based formation control methods, which forces uninterrupted communication among spacecraft. This means that each spacecraft needs to exchange information with its neighbors at every sampling instant. Actually, when the measurement output changes only slightly in some time intervals, information transmission can be unnecessary, otherwise some redundant data packets that need to waste communication resources for transmission will be generated. In practice, the communication between spacecraft is usually based on wireless network, which makes its communication bandwidth limited. Especially for small spacecraft with power-limited communication equipments, the uninterrupted information transmission will cause the overutilization of communication resources and adversely affect the control of SFF system[24,25]. Event-triggered mechanism (ETM) can alleviate the pressure on the communication network by reducing the frequency of information transmission between formation members, so it can perfectly circumvent the above-mentioned problems[26]. Unlike the existing time-triggered methods, the communication of ETMs depends on a triggering condition (also named as event) related to the system states. Only when the defined condition is met will the formation members transfer information with their neighbors. This non-periodic information exchange successfully avoids unnecessary communication between agents, thereby releasing the pressure of the wireless network. Event-triggered mechanism is also fully applied in the formation controller design of multi-spacecraft system. In 27, an adaptive event-triggered cooperative controller is designed to solve the attitude consensus problem of the SFF system. In 28, a sliding mode controller with a novel triggering condition is proposed to achieve attitude consensus and angular velocity consensus. In 29, the formation reconstruction and maintenance of the six-degree-of-freedom spacecraft with multiple uncertainties as well as communication and computation constraints is considered. Relevant results continue to appear in 30,31 and references therein. However, an ongoing drawback of the ETM is that its aperiodic information transmission may cause degradation of system performance. Therefore, how to balance the desired performance of multi-spacecraft system and the utilization of communication resources is a challenge. Further study of ETM is worthwhile if system performance is guaranteed.

The problem mentioned above can be solved by the prescribed performance control (PPC), which can achieve the pre-specified dynamic and steady-state performance through performance functions and transform errors[32,33,34]. Inspired by the case of funnel

control, the methodology of PPC was first developed in 2008 and has since been widely used in tracking control[35,36,37]. In addition to these routine applications, researchers try to combine the PPC method with the finite-time control, so that the transient performance of the system can be realized more quickly. This combination usually manifests itself in two ways. One is to design a finite-time performance function to improve the transient performance, and the other is to combine the conventional PPC with other finite-time designs to ensure the performance and enhance the robustness of the system. In 38, a finite-time performance function was used to design a controller for pure-feedback system to ensure that the tracking error can converge to a predefined precision within a finite time. In 39, a composite finite-time control was designed for permanent-magnet synchronous motors, in which the PPC was introduced to improve the control performance and a finite-time observer was proposed to estimate the undesired disturbance. Ref. 40 addressed the adaptive dynamic positioning problem of an unmanned surface vehicle by a model-free prescribed performance controller, in which a "softening" sign function is proposed to ensure robustness and finite-time stability. The combination of PPC and finite-time theory is indeed beneficial to system performance. However, there are still two imperfections on the finite-time theory. One is that it converges more slowly than the asymptotic one when the system state is far from the equilibrium point, and the other is that its convergence time depends mainly on the initial conditions or controller gains of the system[41].

Motivated by the above technical gaps, in this paper, an I&I-based event-triggered controller with guaranteed performance is proposed, so as to solve the formation problem of SFF system. Wherein, the I&I control combined with the PPC method is applied to design the formation controller for the whole system. The adaptive I&I technique is introduced to estimate the uncertain parameters during formation phase. Compared with the existing works, this paper possess the following main contributions.

1. The I&I technique is used as a foundation to design the distributed formation tracking controller for multi-spacecraft system. Different from the existing related works, the proposed I&I-based controller, which absorbs the properties of the PPC method the and fixed-time technology, can equivalently turn the tracking problem into a stabilization one through the transform errors. With the designer-specific performance function, the tracking errors can converge to the desired accuracy smoothly within the user-given time, without the need to repeatedly adjust the controller parameters.

2. The event-triggered mechanism is incorporated into the formation controller design. Compared with the existing I&I researches based on continuous sampling, this combination enables information transfer between spacecraft to occur only when needed, greatly reducing the burden on communication resources. Furthermore, an exponential-type artificial potential function is designed to avoid collisions between members during formation.

3. We introduce a linear extended state observer to deal with the parameter uncertainties and external disturbances, and use the adaptive I&I technique to realize the online estimation of observer errors through local and neighbors' information, so as to further improve the system performance. Different from the direct estimation of conventional adaptive control, an auxiliary tuning term is added here. Such design can fully inherit the invariant and attractive properties of the implicit manifold under the I&I control, and show more design freedom in reducing the error of parameter estimation.

The remainder of this paper is structured as follows. In Section 2, the dynamics of the multi-spacecraft system and I&I control are introduced, and the algebraic graph theory and the control objective of this paper are also expounded. Section 3 describes the main results of this paper. The core idea of section 4 is simulation verification. Finally, the conclusion is given in Section 5.

Notations: $\mathcal{R}^l$ and $\mathcal{R}^{l \times m}$ stand for the $l$-dimensional real vector and $l \times m$-dimensional real matrix, respectively. $T, |\cdot|, \|\cdot\|$ refer to the vector transpose, the absolute value of a constant and the Euclidean norm of a vector, respectively. $\boldsymbol{I}_{n \times n}$ represents the $n \times n$ identity matrix, $\boldsymbol{I}_n$ represents the $n$-dimensional vector with element 1. $\boldsymbol{diag}(*)$ is defined as the diagonal matrix.

## 2 | PRELIMINARY

In this paper, we hope to construct an appropriate I&I-based controller to achieve and maintain the desired geometry within the fixed time. To this end, we first introduce some necessary preliminaries.

## 2.1 | I&I control

The essence of I&I technique is to ensure stability by immerging the controlled system into a reduced-order stable target system. Its implementation depends on four steps: finding an appropriate target system, ensuring the existence of the immersion conditions, selecting an implicit manifold, designing a controller to ensure the manifold invariance and attractivity, and trajectory boundedness[22,23].

Consider a controlled system $\dot{x} = f(x) + g(x)u$ with a stable equilibrium point $x_*$, where $x, x_* \in \mathcal{R}^n$, $u \in \mathcal{R}^p$. Suppose there is a constant $m$ that satisfies $m < n$. Assume that we have the following mappings $\alpha_1(\cdot) : \mathcal{R}^m \to \mathcal{R}^m, \pi_1(\cdot) : \mathcal{R}^m \to \mathcal{R}^n, c_1(\cdot) : \mathcal{R}^m \to \mathcal{R}^p, \phi_1(\cdot) : \mathcal{R}^n \to \mathcal{R}^{n-m}, \vartheta_1(\cdot, \cdot) : \mathcal{R}^{n \times m} \to \mathcal{R}^p$. According to the aforementioned four steps, the premise of the I&I technique is to find a stable target system $\dot{\zeta} = \alpha_1(\zeta)$ with a globally asymptotically stable equilibrium point $\zeta_*$, where $\zeta, \zeta_* \in \mathcal{R}^m$, $x_* = \pi_1(\zeta_*)$. Then, we can find the following immersion condition $f(\pi_1(\zeta)) + g(\pi_1(\zeta))\vartheta_1(\pi_1(\zeta)) = \frac{\partial \pi_1}{\partial \zeta}\alpha_1(\zeta)$, for all $\zeta \in \mathcal{R}^m$. Next, an appropriate implicit manifold should be chosen so that the following set identity $\mathcal{M} = \{x \in \mathcal{R}^n | \phi_1(x) = 0\} = \{x \in \mathcal{R}^n | x = \pi_1(\zeta)\}$ holds for some $\zeta \in \mathcal{R}^m$. Finally, a control law is designed to ensure all trajectories of the system $\dot{\mathcal{X}} = \frac{\partial \phi_1}{\partial x}[f(x) + g(x)\vartheta_1(x, \mathcal{X})]$, $\dot{x} = f(x) + g(x)\vartheta_1(x, \mathcal{X})$ are bounded and satisfy $\lim_{t \to \infty} \mathcal{X}(t) = 0$. Then, $x_*$ is the globally asymptotically stable equilibrium of the following system $\dot{x} = f(x) + g(x)\vartheta_1(x, \phi_1(x))$.

## 2.2 | Algebraic graph theory

Consider the multi-spacecraft system with $N$ followers and a virtual leader. These $N + 1$ members are communicated via an undirected graph $\mathcal{G} = (v, \mathcal{E})$, where $v = 0, 1, \cdots, N$ represents the set of $N$ followers (labeled as '1, $\cdots$, N') and the virtual leader (labeled as '0'), $\mathcal{E} \subseteq v \times v$ refers to as the edge set. $(i, j) \in \mathcal{E}$ indicates that there is an edge between the $ith$ and $jth$ followers, that is, information can be exchanged between the two spacecraft. $\mathcal{N}_i$ represents the neighbor set of the $ith$ follower, i.e., $\mathcal{N}_i = \{j \in v | (i, j) \in \mathcal{E}\}$. Neighbors can communicate with each other. $\mathcal{A} = [a_{ij}]_{N \times N}$ represents the adjacency weighted matrix with its element $a_{ij}$. If there is an edge betwwen the $ith$ and the $jth$ spacecraft, $a_{ij} = 1$, otherwise $a_{ij} = 0$. Information exchange cannot occur on a single agent, therefore $a_{ii} = 0$. For an undirected graph, $(i, j) \in \mathcal{E} \Leftrightarrow (j, i) \in \mathcal{E}$ is hold. Furthermore, define the Laplacian matrix as $\bar{\mathcal{L}} = \mathcal{D} - \mathcal{A}$, where $\mathcal{D} = diag(d_1, \cdots, d_N)$ refers to as the degree diagonal matrix and $d_i = \sum_{j \in \mathcal{N}_i} a_{ij}$.

Naturally, there is communication between the virtual leader and followers, but it is one-way. $\mathcal{B} = diag(b_1, \cdots, b_N)$ represents the leader adjacency matrix, where $b_i > 0$ means that the $ith$ follower can get the leader's information, otherwise $b_i = 0$. To facilitate subsequent controller design, it is assumed that at least one follower has access to the leader's information, namely $b_1 + b_2 + \cdots + b_N > 0$.

## 2.3 | Dynamics of the multi-spacecraft system

Assume that the members of the controlled multi-spacecraft system are identical. Let $\mathcal{L} = \{X, Y, Z\}$ refer to as the ECI coordinate frame and $\mathcal{C} = \{x_c, y_c, z_c\}$ stands for the LVLH frame. The schematic of the multi-spacecraft system is given in Figure 1, where a virtual leader is introduced to help followers move from the initial positiosn to the desired formation configuration. Note that the virtual leader is not a real spacecraft, but a virtual one moving on a specific orbit around the earth. $R_c = [R_c, 0, 0]^T$ is the distance vector from the center of the earth, pointing toward the virtual leader, where $R_c = a_c(1 - e_c^2)/(1 + e_c \cos \theta)$. $\theta, a_c, e_c$ are respectively, denoted as the true anomaly, semimajor axis, and orbit eccentricity. Further, we define $p_i = [p_{ix}, p_{iy}, p_{iz}]^T \in \mathcal{R}^3, (i = 1, \cdots n)$ as the position vector of the $ith$ follower with respect to the LVLH frame and $v_i$ as the velocity vector correspondingly. Then, one can obtain the following relevant motion dynamics of the $ith$ follower spacecraft[42].

$$\begin{aligned} \dot{p}_i &= v_i \\ m_i \dot{v}_i + C_i v_i + D_i p_i + n_i &= u_i + d_i \end{aligned} \tag{1}$$

where for the $ith$ spacecraft, $m_i$, $u_i$ and $d_i$ represent its mass, the actual control input and the external disturbance vector, respectively. $C_i = 2m_i[0, -\dot{\theta}, 0; \dot{\theta}, 0, 0; 0, 0, 0]$ refers to as the skew-symmetric matrix. $n_i = m_i \mu [R_c/r_i^3 - 1/R_c^2, 0, 0]^T$ stands for the gravity vector, of which $r_i = \sqrt{[(R_c + p_{ix})^2 + p_{iy}^2 + p_{iz}^2]}$ denotes the distance of the $ith$ follower relative to the center

of the earth. $\mu$ represents the earth's gravitational constant. The term $\boldsymbol{D}_i$ has the following expression.

$$\boldsymbol{D}_i = m_i \begin{bmatrix} \mu/r_i^3 - \dot{\theta}^2 & -\ddot{\theta} & 0 \\ \ddot{\theta} & \mu/r_i^3 - \dot{\theta}^2 & 0 \\ 0 & 0 & \mu/r_i^3 \end{bmatrix} \tag{2}$$

where the first and second derivatives of the true anomaly $\theta$ are respectively denoted as $\dot{\theta} = n_c \left(1 + e_c \cos\theta\right)^2 \big/ \left(1 - e_c^2\right)^{3/2}$ and $\ddot{\theta} = -2n_c^2 e_c \left(1 + e_c \cos\theta\right)^3 \sin\theta \big/ \left(1 - e_c^2\right)^3$ with $n_c = \sqrt{\mu/a_c^3}$ is the leader's mean orbital angular velocity.
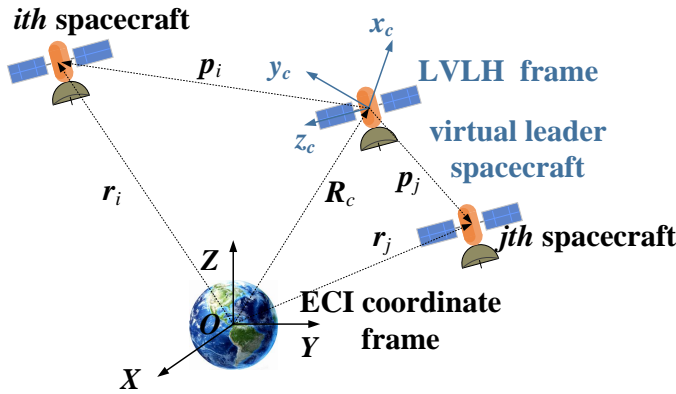


**Figure 1** Schematic of the multi-spacecraft system.
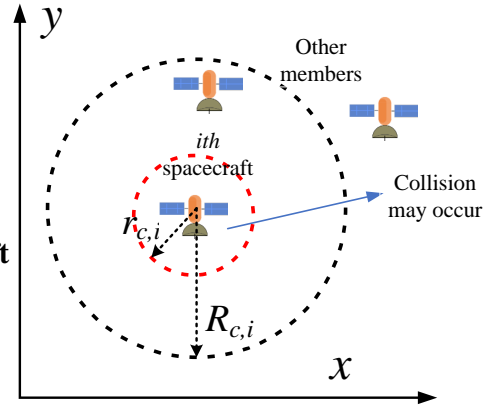
**Figure 2** Two circular regions of the multi-spacecraft system.

Before we proceed, we would like to stress the control objective of this work, which is to design an event-triggered I&I-based formation tracking controller for the multi-spacecraft system to realize high-precision, performance guaranteed and collision-free formation reconstruction within the fixed-time under the aperiodic controller updates.

**Assumption 1** The external disturbance $\boldsymbol{d}_i$ is unknown but bounded, that is, $\|\boldsymbol{d}_i\| \leq d_0$ with $d_0$ is an uncertain positive constant.

# 3 | MAIN RESULTS

In this section, the details of the proposed I&I-based formation tracking controller is presented, and the corresponding stability analysis is explicitly conducted. Because the proposed controller expects to realize formation tracking without internal collisions, the actual control input consists of two parts, as following shows.

$$\boldsymbol{u}_i = \underbrace{\boldsymbol{u}_{i,c}}_{formation\ tracking} + \underbrace{\frac{m_i}{M_i} \cdot \boldsymbol{\eta}_{2,i}^{-1} \boldsymbol{u}_{i,col}}_{collision\ avoidance} \tag{3}$$

where $\boldsymbol{u}_{i,c}$ is designed for formation reconfiguration, $\boldsymbol{u}_{i,col}$ is applied to achieve collision-free formation tracking, $M_i = \sum\limits_{j \in \mathcal{N}_i} a_{ij} + b_i$. The gain coefficient $\frac{m_i}{M_i}$ exists for the convenience of subsequent controller design.

## 3.1 | Design of the collision-avoidance control item

The collision-avoidance control item $\boldsymbol{u}_{i,col}$ is designed to ensure that each spacecraft is always in the safe zone of its neighbors. For this purpose, it can be constructed as the following form.

$$\boldsymbol{u}_{i,col} = k_{c,i} \sum_{j \in \mathcal{N}_i^{col}} -\nabla_{\boldsymbol{p}_i} \Psi_{c,ij}\left(l_{ij}\right) = -k_{c,i} \sum_{j \in \mathcal{N}_i^{col}} \varphi_{c,ij}\left(l_{ij}\right) \frac{\boldsymbol{d}_{ij}}{l_{ij}} \tag{4}$$

where $\nabla_{p_i}$ represents the gradient along $p_i$. The negative sign means that the $ith$ spaceraft exerts a repulsive force on the $jth$ follower that is likely to collide. $k_{c,i}$ is a user-designed positive constant. For the $i$-th follower, $\mathcal{N}_i^{col} = \{j | r_{c,i} \le l_{ij} \le R_{c,i}\}$ stands for its collision-avoidance neighbor. It is worth emphasizing that the two neighbor sets in this paper are different in definition. The collision-avoidance neighbor set $\mathcal{N}_i^{col}$ is only related to distance. And the topology neighbor set $\mathcal{N}_i$ depends on whether information can be directly exchanged between two agents. When $l_{ij} \le r_{c,i}$ holds, it indicates that there is a collision between the formation members. Also, $\Psi_{c,ij}\left(l_{ij}\right) = \int_{r_{c,i}}^{l_{ij}} \varphi_{c,ij}(s)ds$ in $\mathbf{u}_{i,col}$ is called the artificial potential function, and $\varphi_{c,ij}(\cdot)$ is its action function, which has the following form.

$$\varphi_{c,ij}(l_{ij}) = \begin{cases} -\exp\left(\frac{R_{c,i}^2 - l_{ij}^2}{l_{ij}^2 - r_{c,i}^2 + Q_i}\right), & r_{c,i} \le l_{ij} \le R_{c,i} \\ 0 & , otherwise \end{cases} \tag{5}$$

where $\mathbf{d}_{ij} = \mathbf{p}_i - \mathbf{p}_j$ is the position vector of the $ith$ spacecraft with respect to the $jth$ member, and $l_{ij} = \left\|\mathbf{d}_{ij}\right\|$ is the distance between the two members. $r_{c,i}$ and $R_{c,i}$ are the two circular intervals, as shown in Figure 2, called collision zone and safety zone, respectively. $Q_i > 0$ is introduced so that $\varphi_{c,ij}(\cdot)$ is not unbounded. $\varphi_{c,ij}(l_{ij}) \to \infty$ holds if $Q_i$ is small enough and $l_{ij} \to r_{c,i}$.

## 3.2 | Design of the I&I-based formation tracking controller

For the $ith$ follower, assume that $\mathbf{p}_{i,d}$ is defined as the desired position vector relaive to the virtual leader, the corresponding position tracking error can be expressed as $\tilde{\mathbf{p}}_i = \mathbf{p}_i - \mathbf{p}_{i,d}$. Meanwhile, $\mathbf{v}_{i,d}$ is the desired velocity vector, then we have $\dot{\mathbf{p}}_{i,d} = \mathbf{v}_{i,d}$ and $\tilde{\mathbf{v}}_i = \mathbf{v}_i - \mathbf{v}_{i,d}$. Further, let $\mathbf{y}_r$ be the moving trajectory of the formation center in the LVLH frame, and $\mathbf{\Delta}_i$ be the desired position of the $ith$ spacecraft with respect to the formation center. According to the vector addition rule, one can obtain $\mathbf{p}_{i,d} = \mathbf{y}_r + \mathbf{\Delta}_i$. Here we assume that the desired formation configuration is time-invariant, that is, $\mathbf{\Delta}_i$ is constant. Then , based on the above analysis, the global formation tracking error and velocity error can be expressed as

$$\begin{aligned} \mathbf{e}_i &= \sum_{j \in \mathcal{N}_i} a_{ij}(\mathbf{p}_i - \mathbf{p}_j - \mathbf{\Delta}_{ij}) + \bar{b}_i(\mathbf{p}_i - \mathbf{y}_r - \mathbf{\Delta}_i) \\ \mathbf{e}_{v,i} &= \sum_{j \in \mathcal{N}_i} a_{ij}(\mathbf{v}_i - \mathbf{v}_j) + \bar{b}_i(\mathbf{v}_i - \dot{\mathbf{y}}_r) \end{aligned} \tag{6}$$

In order to deal well with the possible unmodeled dynamics and external disturbances, the following extended state observer (ESO) is designed

$$\begin{cases} \dot{z}_{1,i} = z_{2,i} - \bar{\beta}_{1,i}\left(z_{1,i} - \mathbf{p}_i\right) \\ \dot{z}_{2,i} = z_{3,i} - \bar{\beta}_{2,i}\left(z_{1,i} - \mathbf{p}_i\right) + \frac{u_i}{m_i} \\ \dot{z}_{3,i} = -\bar{\beta}_{3,i}\left(z_{1,i} - \mathbf{p}_i\right) \end{cases} \tag{7}$$

where $z_{1,i}, z_{2,i}$ are the estimations of $\mathbf{p}_i$ and $\mathbf{v}_i$, respectively. $z_{3,i}$ is the estimation of the defined extended state $x_{3,i}$ with $x_{3,i} = -\frac{C_i}{m_i} \cdot \mathbf{v}_i - \frac{D_i}{m_i} \cdot \mathbf{p}_i - \frac{n_i}{m_i} + \frac{d_i}{m_i}$. Note that $x_{3,i}$ encapsulates all system uncertainties that may exist. $\bar{\beta}_{k,i}, k = 1, 2, 3$ are the observer gains, satisfying the following polynomials $s^3 + \bar{\beta}_{1,i}s^2 + \bar{\beta}_{2,i}s + \bar{\beta}_{3,i} = (s + \omega_{o,i})^3$, where $\omega_{o,i}$ is the obsever bandwidth. Let $e_{o3,i} = x_{3,i} - z_{3,i}$ be the estimation error of the extended state. The convergence of ESO has been verified in Ref.[43], which will not be described here for brevity. Therefore, $e_{o3,i}$ is bounded and can be estimated by the adaptive technique.

Taking the derivative of (6) with respect to time yields

$$\begin{aligned} \dot{\mathbf{e}}_i &= \mathbf{e}_{v,i} \\ \dot{\mathbf{e}}_{v,i} &= M_i Y_i + \frac{M_i}{m_i} \mathbf{u}_i - b_i \ddot{\mathbf{y}}_r - \sum_{j \in \mathcal{N}_i} a_{ij} \frac{u_j}{m_j} - \sum_{j \in \mathcal{N}_i} a_{ij} Y_j \end{aligned} \tag{8}$$

where $M_i = \sum_{j \in \mathcal{N}_i} a_{ij} + b_i, Y_i = e_{o3,i} + z_{3,i}, Y_j = e_{o3,j} + z_{3,j}$. The purpose of this paper is to achieve the formation tracking within the specified time. Here we hope the convergence time to depend only on the users' requirements, rather than the designed controller parameters or the initial system conditions. Therefore, the SMC-based technique or the previously mentioned fixed-time control will not be applicable. Fortunately, the PPC method provides an available tool for solving this problem. We first apply corresponding boundary constraints to the global errors in (8).

$$-\rho_{1,i} < e_i < \rho_{1,i}, -\rho_{2,i} < e_{v,i} < \rho_{2,i} \tag{9}$$

where $\rho_{1,i}$ and $\rho_{2,i}$, called PPF, are the main factors that determine the transient and steady-state performance of the global errors. Here, in order to enable the error signals to converge within the user-given time, a fixed-time PPF is proposed in the authors' previous work, which can be written as the following form[44].

$$\dot{\rho}_{k,i}(t) = \begin{cases} -p_{k,0}\left(\rho_{k,i}(t) - \rho_{k,\infty}\right)^{\iota_k} & , \text{ if } t \leq T_{f,k} \\ 0 & , \text{otherwise} \end{cases}, k = 1,2 \tag{10}$$

where $p_{k,0} = \left(\left(\rho_{k,0} - \rho_{k,\infty}\right)^{1-\iota_k}\right) / \left((1 - \iota_k)T_{f,k}\right)$, $\iota_k \in (0.5,1) \subseteq \mathcal{R}$, $\rho_{k,0}, \rho_{k,\infty} > 0$ are user-given positive constants. $T_{f,k}$ is the preassigned convergence time.

According to (9), we have

$$-1 < e_i/\rho_{1,i}, e_{v,i}/\rho_{2,i} < 1 \tag{11}$$

Since the additional constraints in (9) increase the difficulty of the controller design, the following one-to-one homeomorphic mapping function is introduced to transform the constrained system (11) into unconstrained one

$$\xi_{1,i} = \ln\frac{1 + e_i/\rho_{1,i}}{1 - e_i/\rho_{1,i}}, \xi_{2,i} = \ln\frac{1 + e_{v,i}/\rho_{2,i}}{1 - e_{v,i}/\rho_{2,i}} \tag{12}$$

Taking the time-derivative of $\xi_{1,i}(t)$ and $\xi_{2,i}(t)$ generates

$$\dot{\xi}_{1,i} = \eta_{1,i}\left(e_{v,i} - \frac{\dot{\rho}_{1,i}}{\rho_{1,i}}e_i\right), \dot{\xi}_{2,i} = \eta_{2,i}\left(\dot{e}_{v,i} - \frac{\dot{\rho}_{2,i}}{\rho_{2,i}}e_{v,i}\right) \tag{13}$$

where $\eta_{k,i} \in \mathcal{R}^{3 \times 3}$, $k = 1,2$ are diagonal matrices with the element $\eta_{k,i,m}$, and $\eta_{1,i,m} = \frac{2}{(1+e_{i,m}/\rho_{1,i})(1-e_{i,m}/\rho_{1,i})}\frac{1}{\rho_{1,i}} > 0$, $\eta_{2,i,m} = \frac{2}{(1+e_{v,i,m}/\rho_{2,i})(1-e_{v,i,m}/\rho_{2,i})}\frac{1}{\rho_{2,i}} > 0$, $e_{i,m}$ and $e_{v,i,m}$ are the $mth(m = 1,2,3)$ elements of $e_i$ and $e_{v,i}$, respectively. According to (12) and (13), the additional constraints in (9) are removed owing to $\xi_{1,i}, \xi_{2,i} \in (-\infty, \infty)$. Therefore, when the designed controller guarantee the boundedness of $\xi_{1,i}, \xi_{2,i}$, the additional constraints can be satisfied, in which case the desired fixed-time stability is achieved.

Since the designed formation controller is based on the I&I technique, the four steps mentioned in section 2.1 should be followed. Before we proceeded, the following mapping functions are given: $\alpha_i(\cdot), \Pi_i(\cdot), c_i(\cdot), \phi_i(\cdot), \vartheta_i(\cdot, \cdot)$. We first define a reduced-order and asymptotically stable target system.

$$\dot{\zeta}_i = -\sigma_i\zeta_i \tag{14}$$

where $\zeta_i \in \mathcal{R}^3$ represents the states of the target system, $\sigma_i$ is a user-decided positive constant. Apparently, the origin is an asymptotically stable equilibrium point of the target system. Then, construct a mapping between the global error system (8) and the target system (13) as $\Pi_i\left(\zeta_i\right) = \left[\zeta_i, \pi_{2,i}\left(\zeta_i\right)\right]^T$, where $\pi_{2,i}(\cdot)$ is a function to be designed. Then, we can get the immersion condition as

$$\begin{aligned} \pi_{2,i}\left(\zeta_i\right) &= -\sigma_i\zeta_i \\ \frac{\partial\pi_{2,i}}{\partial\zeta_i}\left(-\sigma_i\zeta_i\right) &= M_i x_{3,i} + \frac{M_i}{m_i}c_i\left(\Pi_i(\zeta_i)\right) - b_i\ddot{y}_r - \sum_{j\in\mathcal{N}_i}a_{ij}\frac{c_j(\Pi_j(\zeta_j))}{m_j} - \sum_{j\in\mathcal{N}_i}a_{ij}x_{3,j} \end{aligned} \tag{15}$$

Then, we have $\pi_{2,i}\left(\zeta_i\right) = -\sigma_i\zeta_i$, that is, $\pi_{2,i}\left(e_i\right) = -\sigma_i e_i$. In this way, an implicit manifold can be obtained as $\bar{\mathcal{M}}_i = \left\{\phi_i(E_i) = 0\right\} = \left\{e_{v,i} = \pi_{2,i}\left(\zeta_i\right), E_i = \left[e_i^T, e_{v,i}^T\right]^T\right\}$.

One of limitations, in existing related works, is that most I&I-based controls can only guarantee asymptotic convergence of tracking errors, consistent with the performance of the target system. What's worse, the transient and steady-state behaviors of the controlled system can only be guaranteed by repeated tuning of controller parameters, which requires a large amount of time consumption. For this end, we introduce a fixed-time PPC to break these gaps. Through a one-to-one mapping, the initial error system (8) is transformed into the form shown in (13). Detailedly, a modified implicit manifold is defined as the following form.

$$\mathcal{Z}_i = \xi_{2,i} + \sigma_i\xi_{1,i} \tag{16}$$

Accordingly, we can design the following distributed I&I formation tracking controller as

$$U_i = \frac{m_i}{M_i} \cdot \left( \begin{array}{l} k_{i,1}\mathcal{Z}_i + k_{i,2}\eta_{2,i}^{-1}\mathcal{Z}_i + M_i z_{3,i} - b_i\ddot{y}_r - \sum_{j\in\mathcal{N}_i}a_{ij}\frac{u_j}{m_j} - \sum_{j\in N_i}a_{ij}z_{3,j} - \sum_{j\in\mathcal{N}_i}a_{ij}e_{o3,j} \\ +M_i e_{o3,i} - \frac{\dot{\rho}_{2,i}}{\rho_{2,i}}e_{v,i} + \sigma_i\eta_{2,i}^{-1}\eta_{1,i}\left(e_{v,i} - \frac{\dot{\rho}_{1,i}}{\rho_{1,i}}e_i\right) + \frac{M_i}{m_i}\left(1 - \lambda_{1,i}\right)^{-1}\lambda_{2,i}I_3 \end{array} \right) \tag{17}$$

where $k_i > 0$ is the controller gain to be designed. Note that the observer errors should not be ignored in controller design, otherwise it may cause the performance degradation of the system. It should be stressed here that in order to facilitate subsequent approximation, the observer errors are assumed to be slow time-varying compared to the system states. Define $\theta_i$ as the total estimation error, then we have $\theta_i = \sum_{j \in \mathcal{N}_i} a_{ij} e_{o3,j} - M_i e_{o3,i}$. In adaptive I&I technique, an auxiliary regulation term $\beta$ is added to the adaptive law, which provides greater design freedom for improving the estimation accuracy. In this way, $\hat{\theta}_i + \beta_i$ is the estimation of $\theta_i$, and the corresponding estimation error can be defined as the following form.

$$\tilde{\theta}_i = \hat{\theta}_i + \beta_i \left( \xi_{1,i}, \xi_{2,i} \right) - \theta_i \tag{18}$$

Taking the time-derivative of $\tilde{\theta}_i$ yields

$$\dot{\tilde{\theta}}_i = \dot{\hat{\theta}}_i + \frac{\partial \beta_i}{\partial \xi_{1,i}} \cdot \dot{\xi}_{1,i} + \frac{\partial \beta_i}{\partial \xi_{2,i}} \cdot \dot{\xi}_{2,i} = \dot{\hat{\theta}}_i + \frac{\partial \beta_i}{\partial \xi_{1,i}} \cdot \eta_{1,i} \left( e_{v,i} - \frac{\dot{\rho}_{1,i}}{\rho_{1,i}} e_i \right) + \frac{\partial \beta_i}{\partial \xi_{2,i}} \cdot \eta_{2,i} \left( \dot{e}_{v,i} - \frac{\dot{\rho}_{2,i}}{\rho_{2,i}} e_{v,i} \right) \tag{19}$$

Here for ease of understanding, we can think of $\frac{\partial \beta_i}{\partial \xi_{1,i}}$ and $\frac{\partial \beta_i}{\partial \xi_{2,i}}$ as 3×3-dimensional diagonal matrices with elements $\frac{\partial \beta_{i,m}}{\partial \xi_{1,i,m}}$ and $\frac{\partial \beta_{i,m}}{\partial \xi_{2,i,m}}$, respectively, where $\beta_{i,m}$, $\xi_{1,i,m}$ and $\xi_{2,i,m}$ are the $m$th elements of $\beta_i, \xi_{1,i}$ and $\xi_{2,i}$, respectively. According to (19), the following adaptive law can be designed.

$$\dot{\hat{\theta}}_i = -\frac{\partial \beta_i}{\partial \xi_{1,i}} \cdot \eta_{1,i} \left( e_{v,i} - \frac{\dot{\rho}_{1,i}}{\rho_{1,i}} e_i \right) - \frac{\partial \beta_i}{\partial \xi_{2,i}} \cdot \eta_{2,i} \left( \varepsilon_i + \hat{\theta}_i + \beta_i - \frac{\dot{\rho}_{2,i}}{\rho_{2,i}} e_{v,i} \right) \tag{20}$$

where $\varepsilon_i = M_i z_{3,i} + \frac{M_i}{m_i} u_i - b_i \ddot{y}_r - \sum_{j \in \mathcal{N}_i} a_{ij} \frac{u_j}{m_j} - \sum_{j \in \mathcal{N}_i} a_{ij} z_{3,j}$ Substituting (20) into (19) yields

$$\dot{\tilde{\theta}}_i = -\frac{\partial \beta_i}{\partial \xi_{2,i}} \cdot \eta_{2,i} \tilde{\theta}_i \tag{21}$$

In order to guarantee the convergence of the estimation error $\tilde{\theta}_i$, the auxiliary regulation term $\beta_i$ can be given as

$$\beta_i = \frac{c_{1,i}}{12} \eta_{2,i}^{-2} \xi_{2,i}^3 + \frac{1}{5} c_{2,i} \xi_{1,i}^2 \tag{22}$$

where $c_{1,i}, c_{2,i} > 0$ are user-designed constants. After estimating the total observer error, the formation control input in (17) can be written as follows.

$$U_i = \frac{m_i}{M_i} \cdot \begin{pmatrix} k_{i,1} \mathcal{Z}_i + k_{i,2} \eta_{2,i}^{-1} \mathcal{Z}_i + M_i z_{3,i} - b_i \ddot{y}_r - \sum_{j \in \mathcal{N}_i} a_{ij} \frac{u_j}{m_j} - \sum_{j \in N_i} a_{ij} z_{3,j} - (\hat{\theta}_i + \beta_i) \\ -\frac{\dot{\rho}_{2,i}}{\rho_{2,i}} e_{v,i} + \sigma_i \eta_{2,i}^{-1} \eta_{1,i} \left( e_{v,i} - \frac{\dot{\rho}_{1,i}}{\rho_{1,i}} e_i \right) + \frac{M_i}{m_i} \left( 1 - \lambda_{1,i} \right)^{-1} \lambda_{2,i} I_3 \end{pmatrix} \tag{23}$$

In order to achieve a collision-free formation phase, according to (3), $U_i$ can be expressed as

$$U_i = \frac{m_i}{M_i} \cdot \begin{pmatrix} k_{i,1} \mathcal{Z}_i + k_{i,2} \eta_{2,i}^{-1} \mathcal{Z}_i + M_i z_{3,i} - b_i \ddot{y}_r - \sum_{j \in \mathcal{N}_i} a_{ij} \frac{u_j}{m_j} - \sum_{j \in N_i} a_{ij} z_{3,j} - (\hat{\theta}_i + \beta_i) \\ -\frac{\dot{\rho}_{2,i}}{\rho_{2,i}} e_{v,i} + \sigma_i \eta_{2,i}^{-1} \eta_{1,i} \left( e_{v,i} - \frac{\dot{\rho}_{1,i}}{\rho_{1,i}} e_i \right) + \frac{M_i}{m_i} \left( 1 - \lambda_{1,i} \right)^{-1} \lambda_{2,i} I_3 - \eta_{2,i}^{-1} u_{i,col} \end{pmatrix} \tag{24}$$

The communication of multi-spacecraft system depends on the wireless network, which leads to the limited communication bandwidth. At this point, continuous controller updates may cause communication congestion and increase the probability of packet loss, resulting in problems such as increased latency and power consumption. To solve the problem, in this paper, the event-triggered mechanism is introduced, then the final control input can be given as the following form.

$$u_{i,c} = \begin{cases} -(1 + \lambda_{1,i}) U_i, U_i > 0 \\ -(1 - \lambda_{1,i}) U_i, U_i \le 0 \end{cases}, u_i = u_{i,c} \left( t_k^i \right) \tag{25}$$

where $\lambda_{1,i} < 1$ is a parameter to be designed. $t_k^i$ is the triggering time, which is determined by the following triggering condition.

$$t_{k+1}^i = \inf \left\{ t \in \mathcal{R} | \left\| \bar{\mathcal{E}}_{r,i}(t) \right\| \ge \lambda_{1,i} \left\| u_i(t) \right\| + \lambda_{2,i} \right\} \tag{26}$$

where $\bar{\mathcal{E}}_{r,i}(t) = u_{i,c} - u_i$. $\lambda_{2,i} = \tau_{1,i} \big/ \left( \tau_{2,i} + \tau_{3,i} \sqrt{t} \right)$ is called the triggering threshold with $\tau_{1,i}, \tau_{2,i}, \tau_{3,i} > 0$. Obviously, $\lambda_{2,i}$ is bounded in the whole time domain. Eq.(26) indicates that controller updates occur only when the inequality in (26) is satisfied, which will greatly reduce the controller update frequency and unnecessary communication resource consumption.

**Remark 1.** The essence of the I&I techniques is to construct a mapping, so that the target system with the desired performance can be immersed into the controlled system to ensure its performance. In this way, the fixed-time convergence can be achieved

only if the controller is properly designed. The proposed formation controller provide a new tool for I&I techniques to achieve the non-asymptotic convergence. Here, the PPC method is introduced, so that, based on the transformed error system, the designer can realize the fixed-time convergence only by following the design steps of the conventional I&I-based controller. This further increases the flexibility of controller design. Additionally, in this paper, the fixed-time convergence does not rely on any SMC-based techniques, making the convergence time free from the constraints of initial conditions or controller parameters. A real sense of fixed-time stability is achieved.

**Remark 2.** In this paper, the estimation $\hat{\theta}_i + \beta_i$ is used for compensating the uncertain parameters and optimal the performance of the system. Obviously, compared with the traditional adaptive laws based on the equivalence principle, such design adds an additional compensation term. This changes the estimation of system parameters from the original integral action to the proportional integral one, thus increasing the flexibility of parameters estimation and improving the control performance of the system.

**Remark 3.** Figure 3 gives the structure of the proposed controller. When the event in (26) is triggered, the $ith$ formation member broadcasts its current information $u_{i,c}\left(t_k^i\right)$ to its neighbors immediately, and the event-triggered error $\bar{\mathcal{E}}_{r,i}(t)$ is updated to 0 synchronously. Notably, the control input will remain $u_{i,c}\left(t_k^i\right)$ during the event-triggered intervals. If the triggering condition in (26) is not met, there is no communication among the formation members.
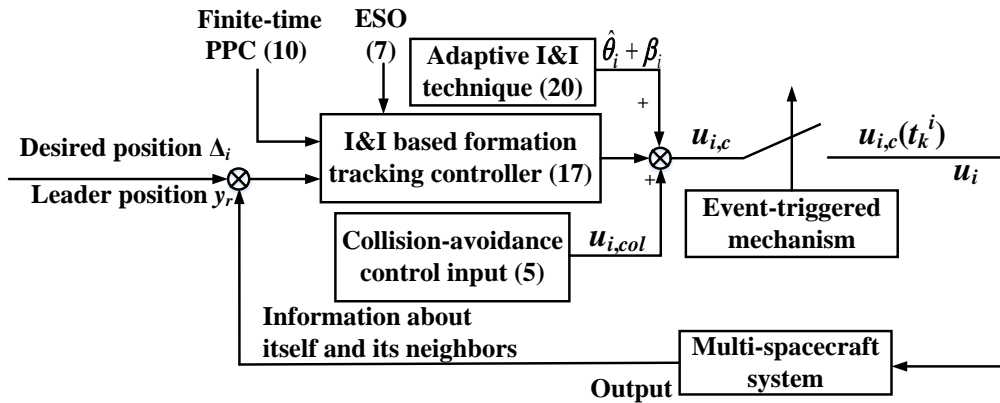


**Figure 3** Structure of the proposed formation controller.

## 3.3 | Stability analysis

Before proceeding, we first summarize the crucial theorem of this work as follows.

**Theorem 1.** Consider the multi-spacecraft system with relative dynamics (1), the collision-avoidance control input (5), the fixed-time PPC technique (10), the adaptive law (20), the formation tracking controller (23)-(25) and the triggering condition (26). If Assumption 1 is valid, then the control objective in 2.3 can be satisfied. Specifically, the desired configuration can be achieved within the user-specfied time, and the bounded constraints in (9) are always satisfied. Also, no collisions occur during formation. Furthermore, Zeno behavior is excluded, that is, the triggering interval is always positive, i.e., $t_{k+1}^i - t_k^i > 0$.

**Proof.** The proof here needs to be considered in three aspects.

1. Convergence of the whole system

According to the triggering condition in (26), we have

$$u_{c,i} = \left(I_{3\times3} + \bar{\lambda}_1(t)\lambda_{1,i}\right)u_i + \bar{\lambda}_2(t)\lambda_{2,i} \tag{27}$$

where $\bar{\lambda}_1 \in \mathcal{R}^{3\times3}, \bar{\lambda}_2 \in \mathcal{R}^3, \left|\bar{\lambda}_{1,m}(t)\right|, \left|\bar{\lambda}_{2,m}(t)\right| \leq 1$ with $\bar{\lambda}_{1,m}(t)$ and $\bar{\lambda}_{2,m}(t)$ are respectively, the $m$th element of $\bar{\lambda}_1$ and $\bar{\lambda}_2$. Eq.(27) can be transformed into the following form.

$$\begin{aligned} u_{c,i} \geq 0, u_i &= \left(1 + \bar{\lambda}_1(t)\lambda_{1,i}\right)^{-1}\left(u_{c,i} - \bar{\lambda}_2(t)\lambda_{2,i}\right) \leq \left(1 - \lambda_{1,i}\right)^{-1}u_{c,i} + \left(1 - \lambda_{1,i}\right)^{-1}\lambda_{2,i}I_3 \\ u_{c,i} < 0, u_i &= \left(1 + \bar{\lambda}_1(t)\lambda_{1,i}\right)^{-1}\left(u_{c,i} - \bar{\lambda}_2(t)\lambda_{2,i}\right) \leq \left(1 + \lambda_{1,i}\right)^{-1}u_{c,i} + \left(1 - \lambda_{1,i}\right)^{-1}\lambda_{2,i}I_3 \end{aligned} \tag{28}$$

Substituting (28) into (25) yields

$$u_i \leq -U_i + (1 - \lambda_{1,i})^{-1} \lambda_{2,i} I_3 \tag{29}$$

Taking the derivative of (16) with respect to time generates

$$\dot{\mathcal{Z}}_i = \dot{\xi}_{2,i} + \sigma_i \dot{\xi}_{1,i} = \eta_{2,i} \left( \dot{e}_{v,i} - \frac{\dot{\rho}_{2,i}}{\rho_{2,i}} e_{v,i} \right) + \sigma_i \eta_{1,i} \left( e_{v,i} - \frac{\dot{\rho}_{1,i}}{\rho_{1,i}} e_i \right)$$
$$= \eta_{2,i} \left( M_i Y_i + \frac{M_i}{m_i} u_i - b_i \ddot{y}_r - \sum_{j \in N_i} a_{ij} \frac{u_j}{m_j} - \sum_{j \in N_i} a_{ij} Y_j - \frac{\dot{\rho}_{2,i}}{\rho_{2,i}} e_{v,i} \right) + \sigma_i \eta_{1,i} \left( e_{v,i} - \frac{\dot{\rho}_{1,i}}{\rho_{1,i}} e_i \right) \tag{30}$$

According to (24), (29) and (30), one can obtain

$$\dot{\mathcal{Z}}_i \leq \eta_{2,i} \left( -k_{i,1} \mathcal{Z}_i - k_{i,2} \eta_{2,i}^{-1} \mathcal{Z}_i + \tilde{\theta}_i + \eta_{2,i}^{-1} u_{i,col} \right) \tag{31}$$

We first define the Lyapunov function as $V_{i,1} = \frac{1}{2} \tilde{\theta}_i^T \tilde{\theta}_i$ to verify the convergence of the estimation error. Then taking the time-derivative of it, we have

$$\dot{V}_{i,1} = \tilde{\theta}_i^T \dot{\tilde{\theta}}_i \leq -\frac{c_{1,i}}{4} \|\eta_{2,i}\|^{-1} \|\tilde{\theta}_i\|^2 \|\xi_{2,i}\|^2 \leq 0 \tag{32}$$

Eq.(32) shows that $\tilde{\theta}_i$ is a bounded variable, and will converge to the origin asymptotically.

To facilitate the convergence analysis of the whole system, a Lyapunov function is defined as $V_i = \frac{1}{2} \mathcal{Z}_i^T \mathcal{Z}_i + V_{i,1}$. Then taking the time-derivative of it generates

$$\dot{V}_i = \mathcal{Z}_i^T \dot{\mathcal{Z}}_i + \dot{V}_{i,1} \leq -k_{i,1} \|\eta_{2,i}\| \|\mathcal{Z}_i\|^2 - k_{i,2} \|\mathcal{Z}_i\|^2 + \|\mathcal{Z}_i\| \|\eta_{2,i}\| \|\tilde{\theta}_i\| + \mathcal{Z}_i^T u_{i,col} + \dot{V}_{i,1} \tag{33}$$

According to the Young's inequality, one can obtain $\|\eta_{2,i}\| \|\mathcal{Z}_i\| \|\tilde{\theta}_i\| \leq \frac{1}{2\varpi_1} \|\tilde{\theta}_i\|^2 + \frac{\varpi_1}{2} \|\eta_{2,i}\|^2 \|\mathcal{Z}_i\|^2$ with $\varpi_1 > 0$. Then we plug it into (33) yields

$$\dot{V}_i = \mathcal{Z}_i^T \dot{\mathcal{Z}}_i + \dot{V}_{i,1} \leq - \left( k_{i,1} - \frac{\varpi_1}{2} \|\eta_{2,i}\| \right) \|\eta_{2,i}\| \|\mathcal{Z}_i\|^2 - k_{i,2} \|\mathcal{Z}_i\|^2 + \frac{1}{2\varpi_1} \|\tilde{\theta}_i\|^2 + \mathcal{Z}_i^T u_{i,col} + \dot{V}_{i,1} \tag{34}$$

Reviewing the definition of the collision-avoidance control item in (5), we have the conclusion that when the distance between any two spacecraft is more than $R_{c,i}$, $u_{i,col} = 0$ is workable, and then $\mathcal{Z}_i^T u_{i,col} = 0$. Since the main purpose of this work is to achieve and maintain the desired geometry, this means that each spacecraft stays in the region $\Theta_{ij} = \{l_{ij} | r_{c,i} \leq l_{ij} \leq R_{c,i}\}$ only for a short time. Then, for continuous systems such as the spacecraft, $\mathcal{Z}_i$ is bounded during this short residence time, meaning that $\mathcal{Z}_i^T u_{i,col}$ is also bounded. In conclusion, $\mathcal{Z}_i^T u_{i,col}$ is bounded at all time domain. Additionally, $\tilde{\theta}_i$ is asymptotically convergent, which means we have $\left| \frac{1}{2\varpi_1} \|\tilde{\theta}_i\|^2 + \mathcal{Z}_i^T u_{i,col} \right| \leq \mathcal{A}_i$ with $\mathcal{A}_i > 0$ is an unknown costant. Then according to (34), as long as the choice of $k_{i,1}$ satisfies $k_{i,1} > \frac{\varpi_1}{2} \|\eta_{2,i}\|$, one can obtain

$$\dot{V}_i = \mathcal{Z}_i^T \dot{\mathcal{Z}}_i + \dot{V}_{i,1} \leq -C_i V_i + \mathcal{A}_i \tag{35}$$

where $C_i = 2min \left\{ k_{i,2}, \frac{c_{1,i}}{4} \|\eta_{2,i}\|^{-1} \|\xi_{2,i}\|^2 \right\}$. Eq.(35) indicates that $\mathcal{Z}_i$ is a bounded signal. According to this, the convergence of the transformed error signals can be analyzed.

Here we use the proof by contradiction. For a bounded signal $\mathcal{Z}_i$, assume that $e_i$ is unbounded, then $e_{v,i}$ is also unbounded according to (8). Since $\rho_{1,i}$ and $\rho_{2,i}$ are bounded by definition, it follows from (12) that unbounded $e_i$ and $e_{v,i}$ lead to unbounded $\xi_{1,i}$ and $\xi_{2,i}$. Then, according to (16), $\mathcal{Z}_i$ is unbounded, which contradicts the fact. So, $e_i$ and $e_{v,i}$ are bounded signals. Moreover, considering the fact that the mapping $F_1 : e_i/\rho_{1,i} \to \xi_{1,i}$, $F_2 : e_{v,i}/\rho_{2,i} \to \xi_{2,i}$ are homeomorphous, then the bounded $e_i$ and $e_{v,i}$ means that $\xi_{1,i}$ and $\xi_{2,i}$ are also bounded. Therefore, according to the property of the fixed-time PPC technique, the global error signals $e_i$ and $e_{v,i}$ can converge to the prescribed region within the user-specified time and the desired formation configuration can also be achieved and preserved.

2. Collision-avoidance performance analysis

Here we will validate that no collision occurrs between the $i$-th spacecraft and its neighbor $j(j \in \mathcal{N}_i^{col})$ during formation, so define the a Lyapunov-like function as

$$E_i(t) = \frac{1}{2} d_{ij}^T d_{ij} + \frac{1}{2} v_i^T v_i \tag{36}$$

Taking the time-derivative of $E_i(t)$ and substituting $u_i = u_{i,c} + \frac{m_i}{M_i} u_{i,col}$ into it generates

$$\dot{E}_i(t) = d_{ij}^T \dot{d}_{ij} + v_i^T \dot{v}_i = d_{ij}^T (\dot{p}_i - \dot{p}_j) + v_i^T \left( x_{3,i} + \frac{M_i}{m_i} u_i \right)$$
$$= d_{ij}^T (v_i - v_j) + v_i^T \left( x_{3,i} + \frac{M_i}{m_i} u_{i,c} \right) + \left( -k_{c,i} v_i^T \sum_{j \in \mathcal{N}_i^{col}} \varphi_{c,ij} (l_{ij}) \frac{d_{ij}}{l_{ij}} \right) \tag{37}$$

In the analysis of the first step, we know that $\boldsymbol{u}_{i,c}$, $\boldsymbol{p}_i$ and $\boldsymbol{p}_j$ are all bounded signals. Also, according to the definition of the designed collision-avoidance potential function, when $l_{ij} \to r_{c,i}$, $\left( -k_{c,i} \boldsymbol{v}_i^T \sum_{j \in \mathcal{N}_i^{col}} \varphi_{c,ij} \left( l_{ij} \right) \frac{\boldsymbol{d}_{ij}}{l_{ij}} \right) \to +\infty$ holds if $Q_i$ is small enough. Then, with the appropriate design parameters, we have

$$\left( -\boldsymbol{v}_i^T \sum_{j \in \mathcal{N}_i^{col}} \varphi_{c,ij} \left( l_{ij} \right) \frac{\boldsymbol{d}_{ij}}{l_{ij}} \right) \geq \frac{1}{2} \boldsymbol{d}_{ij}^T \boldsymbol{d}_{ij} + \frac{1}{2} \boldsymbol{v}_i^T \boldsymbol{v}_i - \frac{\boldsymbol{d}_{ij}^T \left( \boldsymbol{v}_i - \boldsymbol{v}_j \right)}{k_{c,i}} - \frac{\boldsymbol{v}_i^T \left( \boldsymbol{x}_{3,i} + \frac{M_i}{m_i} \boldsymbol{u}_{i,c} \right)}{k_{c,i}} \tag{38}$$

From (37) and (38), we have $\dot{E}_i(t) \geq k_{c,i} E_i(t)$. Then according to Lemma 6 in [46], we have the following inequality.

$$\boldsymbol{d}_{ij}^T \boldsymbol{d}_{ij} \geq 2 e^{k_{c,i}(t)} E_i(0) - \boldsymbol{v}_i^T \boldsymbol{v}_i \tag{39}$$

Note that $\boldsymbol{v}_i^T \boldsymbol{v}_i$ is bounded. Therefore, when $k_{c,i}$ is large enough, under a suitable initial state, the inequality $2 e^{k_{c,i}(t)} E_i(0) - \boldsymbol{v}_i^T \boldsymbol{v}_i > \left( r_{c,i} \right)^2$ can be obtained, that is, $\left\| \boldsymbol{d}_{ij} \right\| > r_{c,i}$. It indicates that the internal collisions can be effectively avoided by the designed collision-avoidance control input in (5).

3. Zeno behavior

According to the event-triggered mechanism in (26), we have $\bar{\mathcal{E}}_{r,i}(t) = \boldsymbol{u}_{i,c} - \boldsymbol{u}_i$. We know that when $t \in \left[ t_k^i, t_{k+1}^i \right)$, $\boldsymbol{u}_i = \boldsymbol{u}_{i,c} \left( t_k^i \right)$, that is, $\dot{\boldsymbol{u}}_i(t) = 0$. In this case, $\dot{\bar{\mathcal{E}}}_{r,i}(t) = \dot{\boldsymbol{u}}_{i,c}$ for $t \in \left[ t_k^i, t_{k+1}^i \right)$. Then, $\frac{d}{dt} \left\| \bar{\mathcal{E}}_{r,i}(t) \right\|^2 = 2 \bar{\mathcal{E}}_{r,i}^T \dot{\bar{\mathcal{E}}}_{r,i} = 2 \bar{\mathcal{E}}_{r,i}^T \dot{\boldsymbol{u}}_{i,c}$. According to the analysis in step 1, we known that $\boldsymbol{u}_{i,c}$ is a bounded signal, therefore, $\bar{\mathcal{E}}_{r,i}$ and $\dot{\boldsymbol{u}}_{i,c}$ are all bounded, that is, $\frac{d}{dt} \left\| \bar{\mathcal{E}}_{r,i}(t) \right\|^2 \leq \mathcal{B}_i$ with $\mathcal{B}_i$ is an unknown positive constant. Then the following inequality

$$\left\| \bar{\mathcal{E}}_{r,i} \right\|^2 \leq \int_{t_k^i}^{t} \mathcal{B}_i dt = \mathcal{B}_i \left( t - t_k^i \right) \tag{40}$$

is always satisfied. Therefore, we have

$$\mathcal{B}_i \left( t - t_k^i \right) \geq \left( \lambda_{1,i} \left\| \boldsymbol{u}_i(t) \right\| + \lambda_{2,i} \right)^2 = t^* > 0 \tag{41}$$

where $t^*$ is the lower bound. Eq.(41) indicates that $t - t_k^i \geq \frac{t^*}{\mathcal{B}_i} > 0$. Therefore, Zeno-behavior can be successfully circumvented. $\square$

**Remark 4.** Considering the real flight scenario of the spacecraft, $\boldsymbol{u}_i(t)$ is required here not to exceed its amplitude, that is $\left| u_{i,m}(t) \right| \leq \mathcal{U}_i$, where $u_{i,m}$ is the $m$th element of $\boldsymbol{u}_i(t)$ and $\mathcal{U}_i$ represents the amplitude. When the controller is properly designed, the time that $\boldsymbol{u}_i(t)$ stays at its amplitude is extremely short. During the short dwell time, all the variables of the closed-loop system can be considered bounded, that is, $\mathcal{Z}_i$ is bounded, i.e., $\xi_{1,i}$ and $\xi_{2,i}$ are also bounded. It indicates that the fixed-time convergence can be also guaranteed when the control input reaches its amplitude.

**Remark 5.** The proposed protocol can be extended to the formation tracking control for configuration switching. Note that the configuration switching here refers only to the change of the desired formation shape, not to the communication topology between formation members. In order to ensure that the switched configuration can be quickly realized and maintained, it is necessary to make corresponding changes to the performance function so that the output error is always constrained within the prescribed boundaries.

# 4 | SIMULATION ANALYSIS

In this section, different simulations will be constructed to further verify the performance of the proposed controller. The multi-spacecraft system with 4 followers and a virtual leader is considered. The purpose of this paper is to realize formation reconstruction by moving each member from any position to the desired geometry configuration. Figure 4 gives the communication topology among formation members.

Note that configuration switching is implemented in the simulation. Here we assume that the virtual leader is always moving in an elliptical orbit with $a_c = 7178\,km$, $e_c = 0.01$ and $\theta(0) = 0\,rad$. The gravitational constant is set as $\mu = 3.986 \times 10^{14}\,m^3/s^2$. Each spacecraft here weighs $100\,kg$, i.e., $m_i = 100\,kg$. Additionally, due to the limitations of actual physical conditions, the thrust generated by the spacecraft is not infinite, that is, the control input has a amplitude constraint, assumed to be $10\,N$ [42]. Furthermore, in the simulation, it is assumed that there will be external disturbances during the formation, that is,

$d_i = 0.05[sin(t/10), cos(t/15), sin(t/20)]^T N$, $(i = 1, \cdots, 6)$. Consider the change of the desired configuration. If the simulation time is less than 300 seconds, we set the desired configuration to a square, i.e., $\delta_1 = [20, 20, 10]^T$, $\delta_2 = [20, -20, 10]^T$, $\delta_3 = [-20, -20, 5]^T$, $\delta_4 = [-20, 20, 5]^T$. For the remainder of the simulation, the desired configuration is switched to a trapezoid, i.e., $\delta_1 = [50, 20, -10]^T$, $\delta_2 = [50, -20, -10]^T$, $\delta_3 = [-50, -50, -20]^T$, $\delta_4 = [-50, 50, -20]^T$. Other necessary conditions for simulation are presented in Table 1.
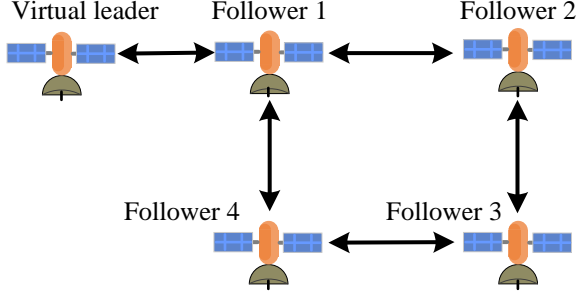


**Figure 4** Communication topology among formation members.

**Table 1** Necessary conditions for simulation.

| Parameters | Values |
|---|---|
| Initial conditions | $p_1(0) = [20, -20\sqrt{2}, 10\sqrt{2}]^T m$ |
| | $p_2(0) = [-15\sqrt{2}, -30\sqrt{2}, 40]^T m$ |
| | $p_3(0) = [-10\sqrt{3}, -20\sqrt{2}, 20]^T m$ |
| | $p_4(0) = [10, -10, -15\sqrt{2}]^T m$ |
| | $v_i(0) = [0, 0, 0]^T m/s (i = 1, \cdots, 4)$ |
| Other conditions | $y_r = [0.5t, 0.5t, 0]^T$, $\dot{y}_r = [0.5, 0.5, 0]^T$ |

**Table 2** Controller parameters of the three examples.

| Examples | Controller parameters |
|---|---|
| Proposed controller | $\rho_{1,0} = 500, \rho_{1,\infty} = 2, \iota_1 = 0.6, \rho_{2,0} = 20, \rho_{2,\infty} = 0.1, \iota_2 = 0.6, T_{f,1} = 80, T_{f,2} = 100, k_{i,1} = 1, k_{i,2} = 0.01$ <br> $k_{c,i} = 0.01, \sigma_i = 1.5, c_{1,i} = 0.05, c_{2,i} = 0.05, \tau_{1,i} = \tau_{2,i} = \tau_{3,i} = 0.1, \lambda_{1,i} = 0.01, \omega_{o,i} = 10$ |
| Example 1 | $\rho_{1,0} = 500, \rho_{1,\infty} = 8, \kappa_1 = 0.04, \rho_{2,0} = 40, \rho_{2,\infty} = 0.1, \kappa_2 = 0.04, k_{i,1} = k_{i,2} = 0.01$ <br> $k_{c,i} = 0.001, \sigma_i = 1.5, c_{1,i} = 0.05, c_{2,i} = 0.05, \lambda_{1,i} = 0.01, \lambda_{2,i} = 0.1 \omega_{o,i} = 10$ |
| Example 2 | $\rho_{1,0} = 400, \rho_{1,\infty} = 5, \iota_1 = 0.55, T_{f,1} = 140, \rho_{2,0} = 20, \rho_{2,\infty} = 0.1$ <br> $\iota_2 = 0.6, T_{f,2} = 120, k_{i,1} = 2, k_{i,2} = 1, k_{c,i} = 0.001, \omega_{o,i} = 10$ |

## 4.1 | Performance verification

We first need to exhibit the performance of the proposed controller, whose design parameters are shown in Table 2. The two circular intervals are chosen as $r_{c,i} = 22$, $R_{c,i} = 35$. Simulation results are shown in Figures 5-13, including the global formation tracking errors and the velocity errors, relative distances between spacecraft with/without collision avoidance, the control inputs of the proposed controller, the estimation errors under the adaptive I&I techniques, the inter-execution intervals of each spacecraft and the moving trajectories of the four formation members.

Results show that with resort to the PPC method, the global error signals are always confined within the constrained boundaries defined by PPFs, which ensure their fixed-time convergence and enable the proposed I&I-based formation tracking controller to realize and maintain the desired geometry configuration within the user-given time. Also, although configuration switching occurs, the proposed protocol can still track the formation shape rapidly and accurately within the pre-appointed time. Moreover, the designed event-triggered mechanism can make the controller update only at the required time, rather than the conventional continuous/periodic update, thus reducing the probability of communication congestion and packet loss, eliminating unnecessary power consumption, and further realizing the full utilization of limited resources. Also, the Zeno-behavior is effectively excluded. Specifically, as shown in Figures 11 and 12, the designed event-triggered mechanism can reduce communication resource consumption by up to 91.4%, which is extremely useful for spacecraft with limited communication bandwidth. Figures 7 and 8 validate that the designed collision-avoidance potential function can effectively prevent collisions between formation members and ensure a safe formation process. Additionally, Figure 10 indicates that the designed adaptive I&I technique can
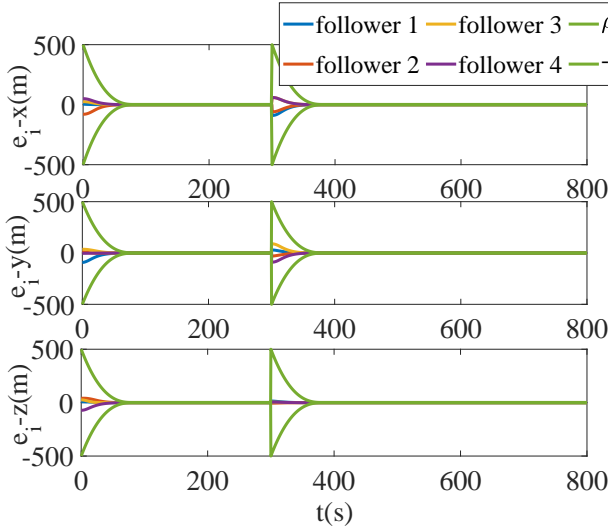
**Figure 5** Global formation errors of the proposed controller. **Figure 6** Global velocity errors of the proposed controller.
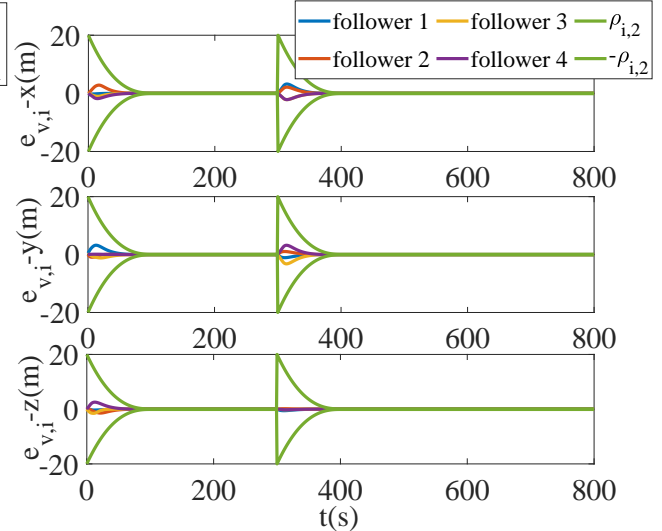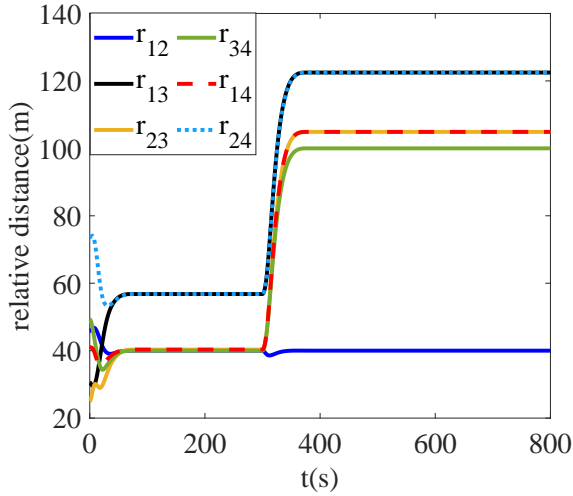


**Figure 7** Relative distance with collision avoidance. **Figure 8** Relative distance without collision avoidance.
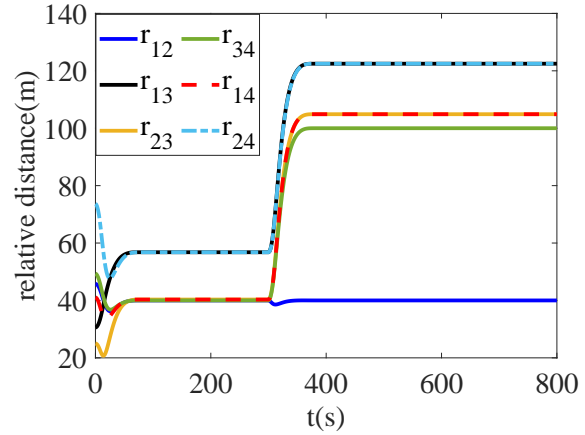
estimate the unknown system arameters timely and accurately. In summary, the proposed controller provide a new tool for I&I-based technique to achieve a true sense of fixed-time stability.

## 4.2 | Performance comparison

In this part, the proposed controller with static event-triggered mechanism and conventional exponential- type PPF (Example 1 for short) and a model-free PPC-based method in 47 (also named as Example 2) are chosen as comparison cases to further verify the superiority of the proposed controller. Configuration switching ia also considered here. In example 1, the threshold $\lambda_{2,i}$ in (26) is a user-designed positive constant and the PPFs are construced as $\rho_{1,i} = (\rho_{1,0} - \rho_{1,\infty}) e^{-\kappa_1 t} + \rho_{1,\infty}, \rho_{2,i} = (\rho_{2,0} - \rho_{2,\infty}) e^{-\kappa_2 t} + \rho_{2,\infty}$ with $\kappa_1, \kappa_2$ decides the convergence rate of the PPF. For example 2, owing to the different model dynamics, the developed method in 47 is not directly applicable. In this case, following the design steps in 47, the formation control protocol for the *ith* follower can be designed as $\alpha_i = -k_{i,1} \ln \left[ \left( 1 + \frac{e_i}{\rho_{1,i}} \right) \Big/ \left( 1 - \frac{e_i}{\rho_{1,i}} \right) \right]$, $u_i = m_i \left( -z_{3,i} - k_{i,2} \ln \left[ \left( 1 + \frac{s_i}{\rho_{2,i}} \right) \Big/ \left( 1 - \frac{s_i}{\rho_{2,i}} \right) \right] \right)$ with $s_i = v_i - \alpha_i$. To make it fair, the designed parameters in both examples are also based on the principle of achieving the desired performance, as shown in Table 2. The remaining simulation conditions are the same as the proposed controller. Furthermore, in order to show the performance of the designed controller quantitatively, a comprehensive performance indexes (CPI) is
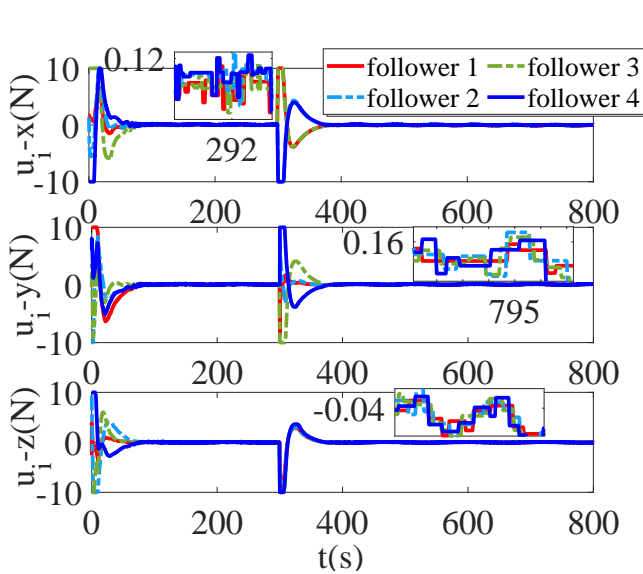
**Figure 9** Control inputs of the proposed controller.
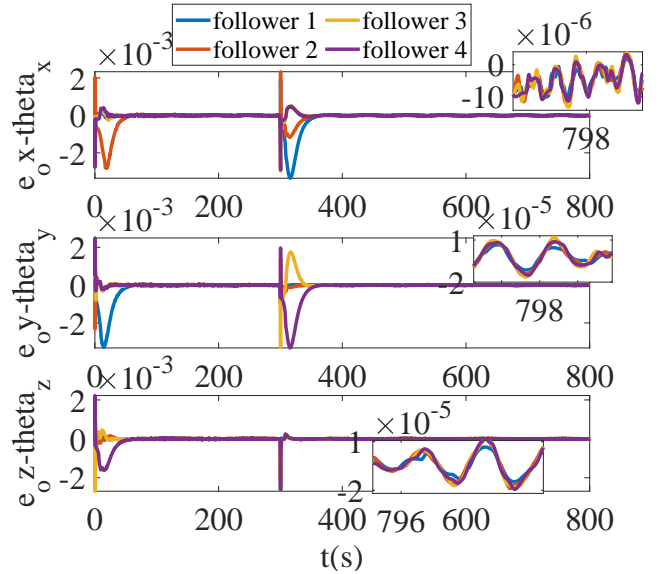


**Figure 10** Estimation errors of the adaptive law.
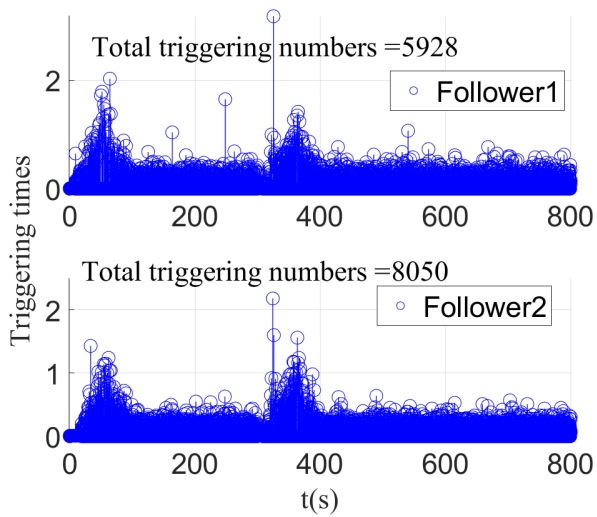


**Figure 11** Inter-execution intervals of each spacecraft.
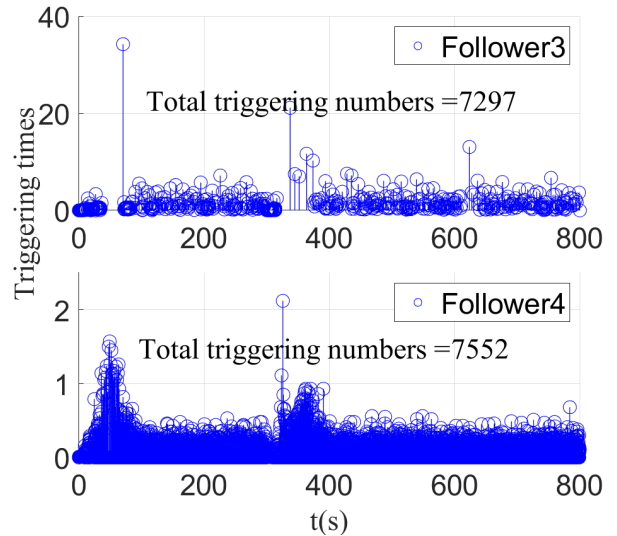


**Figure 12** Inter-execution intervals of each spacecraft.

constructed as $CPI = \left( \sum_{i=1}^{4} \|e_i\|^2 \right)^{1/2}$. Corresponding results are shown in the Figures 14-25 and Table 3, where the convergence time in Table 3 represents the time consumed when $CPI$ converges to 0.01 before and after switching, and '-' indicates that during the simulation time, the global formation tracking errors $e_i$ in example 2 cannot reach the specified precision.

Results show that the two comparison examples can also achieve the desired formation shape. Nevertheless, the proposed protocol still possesses the highest tracking accuracy and the fastest convergence rate among the three techniques, regardless of whether configuration switching occurs, which is also clearly reflected in Table 3. Specifically, the steady-state accuracy of the proposed controller is more than 3 times better than examples 1 and 2, and the convergence time is nearly half of that of example 1. Additionally, in example 1, although the update frequency of the controller under the event-triggered mechanism with constant threshold is reduced by 71.1%, it still consumes more communication resources than the time-varying one in (26). What's more, it can be concluded that, with the aid of the PPC method, the aperiodic controller update of event-triggered mechanism does not cause the system performance degradation, and the fixed-time PPF plays an important role in improving
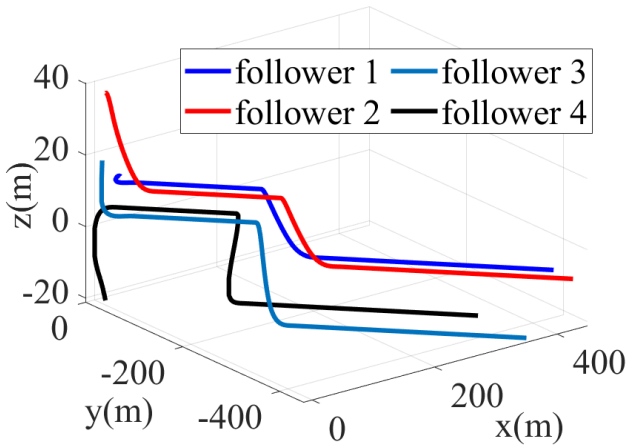
**Figure 13** Moving trajectories under the proposed controller.
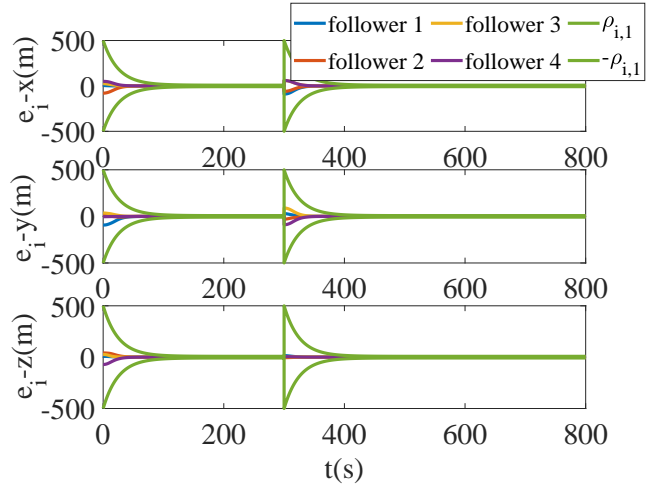


**Figure 14** Global formation errors of the example 1.
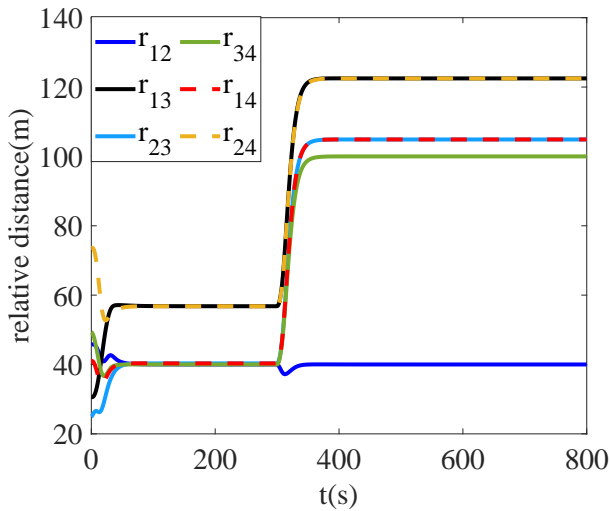


**Figure 15** Relative distance between spacecraft under the example 1.
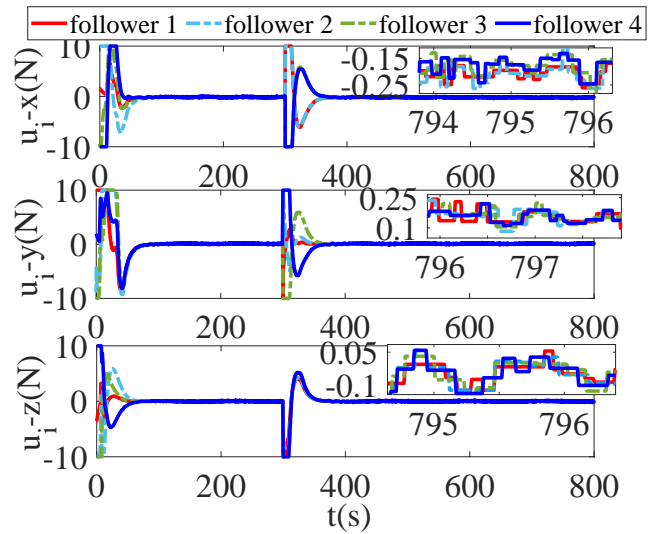


**Figure 16** Control inputs of the system under example 1.

the tracking performance. Moreover, figures 15 and 22 indicates that the proposed collision-avoidance potential function is very flexible and can be applied to many different formation controllers. In summary, the designed controller can find a better balance between communication resource consumption and formation accuracy.

## 5 | CONCLUSIONS

In this paper, a distributed I&I-based formaton tracking controller is constructed for multi-spacecraft system with limited communication capacity, uncertain parameters and external disturbances. Here, by incorporating the strengths of the PPC method and the fixed-time technique, the proposed controller can convert the tracking problem into a stability one via error transformation. Then, relying on the transformed system, the implicit manifold can be designed, in which case the high-precision formation tracking can be achieved within the user-given time by simply following the design steps of the conventional I&I-based controller. To effectively address the problem of communication constraints, the event-triggered mechanism is intruduced to make the controller update only when needed, thus saving resources to the maximum extent. Furthermore, we use the extended state observer to deal with the model uncertainties, and introduce the adaptive I&I technique to estimate the observer errors, so as
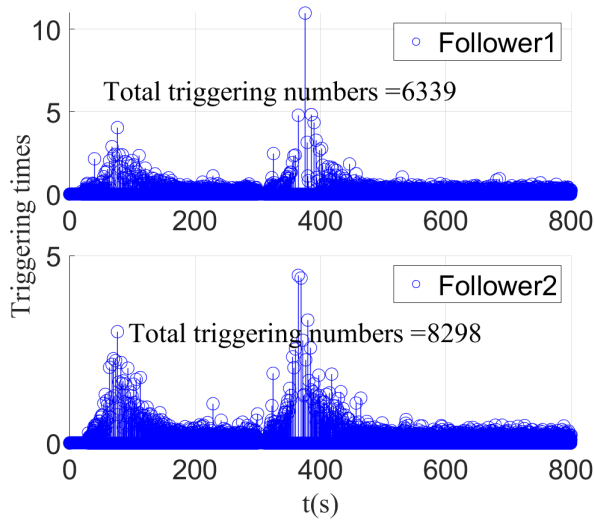
**Figure 17** Inter-execution intervals under example 1.
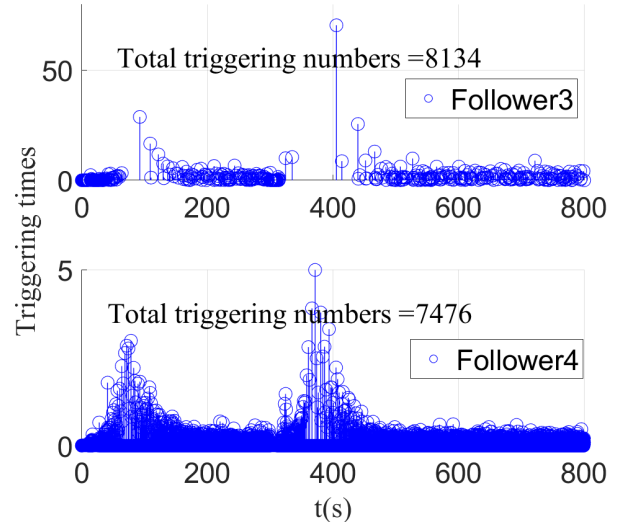


**Figure 18** Inter-execution intervals under example 1.
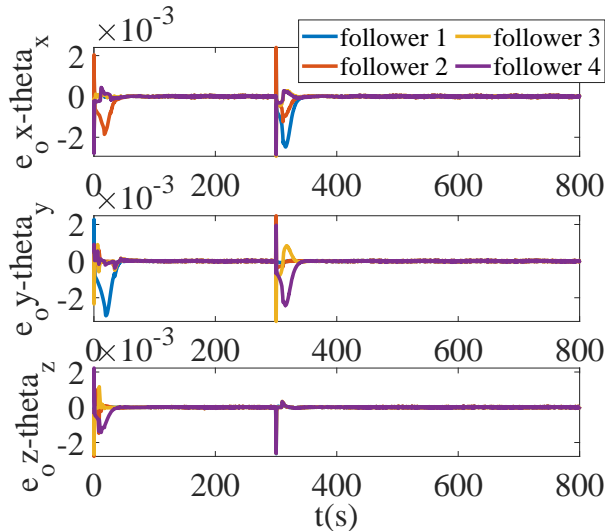


**Figure 19** Estimation errors of the adaptive law under the example 1.
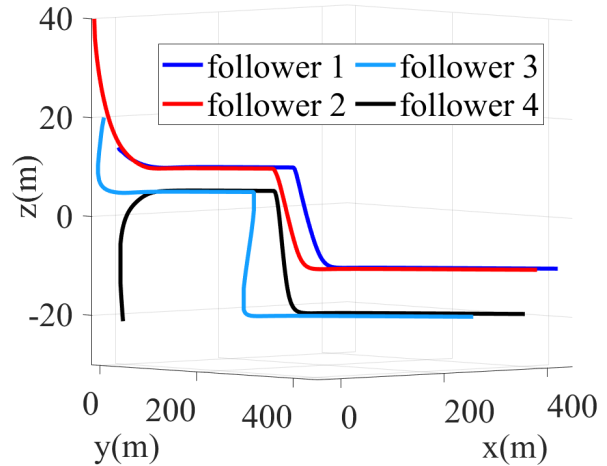


**Figure 20** Moving trajectories under the example 1.

to further improve the performance of the closed-loop system. Finally, the effectiveness of the proposed controller is verified through comparative simulations. Results show that the proposed controller is superior to the two comparison examples in convergence rate (at least 3 times improvement) and tracking accuracy (more than 3 times optimazation). Also, the proposed controller can utilize the limited communication resources more effectively. In conclusion, the designed I&I-based formaton tracking controller can better trade off between resource consumption and convergence accuracy.

# ACKNOWLEDGEMENTS
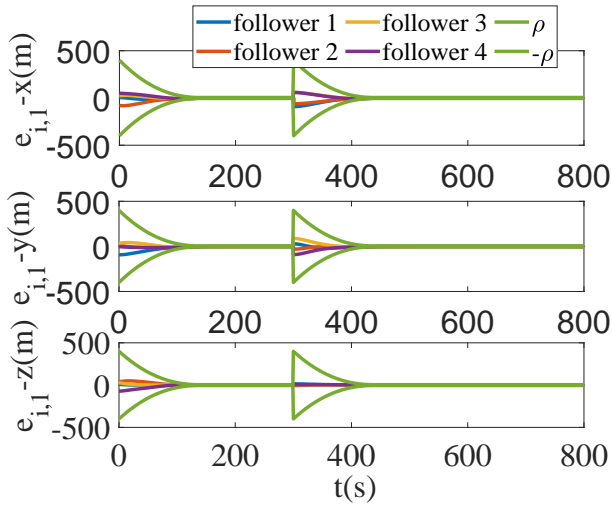
**Figure 21** Formation tracking errors of the example 2.
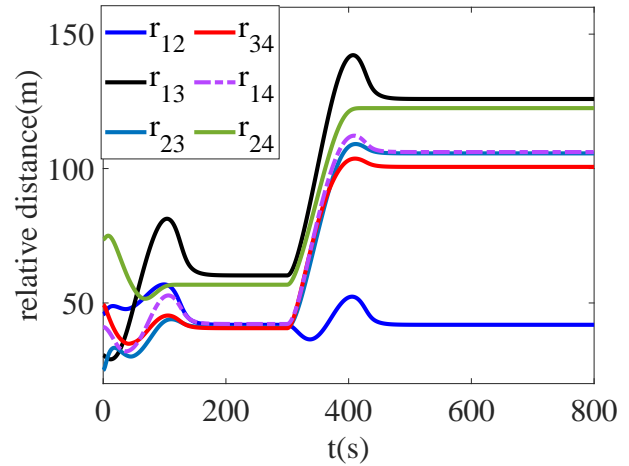


**Figure 22** Relative distances under the example 2.
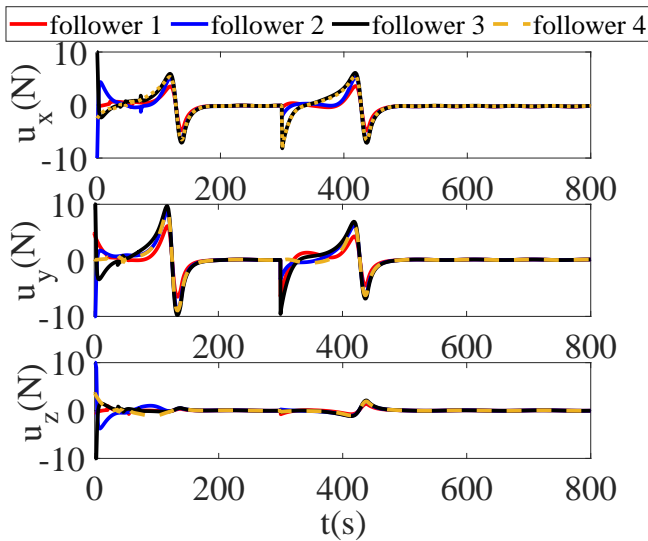


**Figure 23** Control inputs under the example 2.
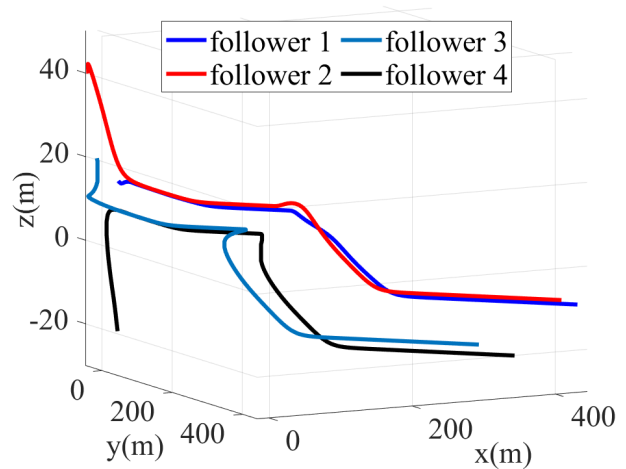


**Figure 24** Moving trajectories under example 2.

# References

1. Hu D, Zhao X, Zhang S. Robust image-based coordinated control for spacecraft formation flying. *Chinese J Aeronaut* 2022; 35(9): 268–281.

2. Lee D. Nonlinear disturbance observer-based robust control for spacecraft formation flying. *Aero Sci Technol* 2018; 76: 82–90.

3. Liu G, Zhang S. A Survey on formation fontrol of small satellites. *Proc IEEE* 2018; 106(3): 440–457.

4. Di M, Lawn M, Bevilacqua R. Survey on guidance navigation and control requirements for spacecraft formation-flying missions. *J Guid Control Dyn* 2018; 41(3): 581–602.
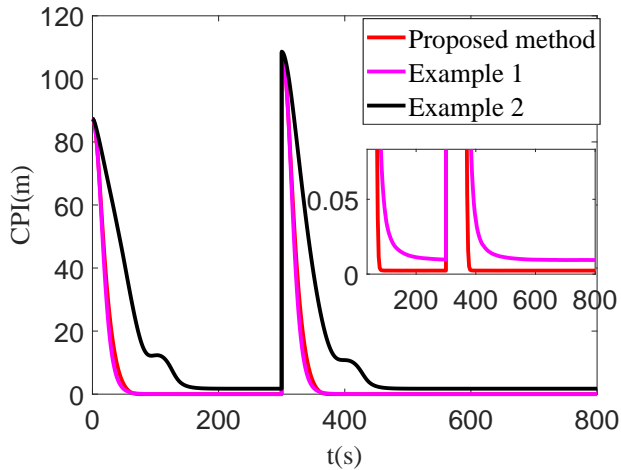
**Figure 25** Time responses of CPI under the three examples.

**Table 3** Performance verification.

| Method | Total triggering number | $|CPI|_{t\to\infty}$ | Convergence time |
|---|---|---|---|
| Proposed | 27583 | 0.0024 | 75/375 |
| Example 1 | 30446 | 0.0094 | 266/557 |
| Example 2 | 320000 | 1.73 | - |

5. Hu Q, Shi Y, CL W. Event-based formation coordinated control for multiple spacecraft under communication constraints. *IEEE Trans Syst Man Cybern Syst* 2021; 51(5): 3168–3179.

6. Jia Q, Gui Y, Wu Y, al e. Disturbance observer-based performance guaranteed fault-tolerant control for multi-spacecraft formation reconfiguration with collision avoidance. *Aero Sci Technol* 2023; 133: 108099.

7. Wu B, DW W, Poh E. Decentralized sliding-mode control for attitude synchronization in spacecraft formation. *Int J Robust Nonlinear Control* 2012; 23(11): 1183–1197.

8. Zhou N, Chen R, Xia Y, al e. Neural networkbased reconfiguration control for spacecraft formation in obstacle environments. *Int J Robust Nonlinear Control* 2018; 28(6): 2442–2456.

9. Gao H, Xia Y, Zhang J, al e. Finite-time fault-tolerant output feedback attitude control of spacecraft formation with guaranteed performance. *Int J Robust Nonlinear Control* 2021; 31(10): 4664–4688.

10. Yang S, Tao G, Jiang B, al e. Modeling and adaptive control of air vehicles with partial nonlinear parametrization. *Automatica* 2023; 149: 110805.

11. Ning X, Yin Y, Wang Z. Unmodeled dynamics suppressed adaptive fault tolerant control for a class of space robots with actuator saturation and faults. *Eur J Control* 2023; 73: 100883.

12. Han C, Liu Z, Yi J. Immersion and invariance adaptive control with $\sigma$-modification for uncertain nonlinear systems. *J Franklin Inst* 2018; 355: 2091–2111.

13. Astolfi A, Ortega R. Immersion and invariance: a new tool for stabilization and adaptive control of nonlinear systems. *IEEE Trans Autom Control* 2003; 48(4): 590–606.

14. Tarek R, Chaouki M, Raoudha B, al e. Adaptive immersion and invariance control for a class of electromechanical systems. In: 2013 International Conference on Electrical Engineering and Software Applications. IEEE. ; March 21–23, 2013; Hammamet, Tunisia.

15. Lu Q, Yu L, Zhang D, al e. An extended immersion and invariance for acceleration-level pseudo-dynamic visual regulation of mobile robots. In: 14th International Conference on Control and Automation. IEEE. ; June 12–15, 2018; Anchorage, Alaska, USA.

16. Zhao B, Xian B, Zhang Y, al e. Nonlinear robust adaptive tracking control of a quadrotor UAV via immersion and invariance methodology. *IEEE Trans Ind Electron* 2015; 62(5): 2891–2902.

17. Jafar K, Mehran H, Javad F, al e. Robust nonlinear control of atomic force microscope via immersion and invariance. *Int J Robust Nonlinear Control* 2019; 29(4): 1031–1050.

18. Fan Y, Jing W, Gao C, al e. Immersion and invariance-based adaptive coordinate control for space manipulator. In: 7th International Conference on Control Science and Systems Engineering. IEEE. ; 30 July–01 August, 2021; Qingdao, China.

19. Zou Y, Meng Z. Immersion and invariance-based adaptive controller for quadrotor systems. *IEEE Trans Syst Man Cybern* 2019; 49(11): 2288–2297.

20. Shao X, Hu Q, Shi Y, al e. Data-driven immersion and invariance adaptive attitude control for rigid bodies with double-level state constraints. *IEEE Trans Control Syst Technol* 2022; 30(2): 779–794.

21. Lou Z, J Z. Immersion-and invariance-based adaptive stabilization of switched nonlinear systems. *Int J Robust Nonlinear Control* 2018; 28(1): 197–212.

22. Yang Y, Song S, Gorbachev S, al e. Distributed adaptive forwarding finite-time output consensus of high-order multia-gent systems via immersion and invariance-based approximator. *IEEE Trans Neural Netw Learn Syst* 2022: 1–15. doi: 10.1109/TNNLS.2022.3203011

23. Yang Y, Song S. Distributed consensus tracking control of a second-order nonlinear multiagent system via immersion and invariance method. *IEEE Syst J* 2022; 16(2): 3120–3129.

24. Meng C, Zhang W, Du X. Finite-time extended state observer based collision-free leaderless formation control of multiple AUVs via event-triggered control. *Ocean Eng* 2023; 268: 113605.

25. Xu C, Wu B, Wang D, al e. Decentralized event-triggered finite-time attitude consensus control of multiple spacecraft under directed graph. *J Franklin Inst* 2021; 358: 9794–9817.

26. Zhu W, Du H, SH L. On event-triggered nonsmooth attitude tracking controller for a rigid spacecraft. *Int J Robust Nonlinear Control* 2022; 32(2): 900–916.

27. Yi H, Liu M, Li M. Event-triggered fault tolerant control for spacecraft formation attitude synchronization with limited data communication. *Eur J Control* 2019; 48: 97–103.

28. Di F, Li A, Guo Y, al e. Event-triggered sliding mode attitude coordinated control for spacecraft formation flying system with disturbances. *Acta Astronautica* 2021; 188: 121–129.

29. Liu Y, Shi M, Li W, al e. Event-triggered prescribed performance control of multi-spacecraft formation with communication and computation constraints. *Aero Sci Technol* 2023; 141: 108506.

30. Chen Z, Wang J, Zhang L, al e. Event-triggered prescribed settling time consensus control of uncertain nonlinear multiagent systems with given transient performance. *ISA T* 2022; 129: 24–35.

31. Wang E, Qiu S, Liu M, al e. Event-triggered adaptive terminal sliding mode tracking control for drag-free spacecraft inner-formation with full state constraints. *Aero Sci Technol* 2022; 124: 107524.

32. Zhang J, Wang Q, Ding W. Global output-feedback prescribed performance control of nonlinear systems with unknown virtual control coefficients. *IEEE Trans Ind Electron* 2022; 67(12): 6904–6911.

33. Jia F, Wang X, Zou X. Robust adaptive prescribed performance control for a class of nonlinear pure-feedback systems. *Int J Robust Nonlinear Control* 2019; 29(12): 3971–3987.

34. Yin Z, Luo J, Wei C. Robust prescribed performance control for EulerLagrange systems with practically finite-time stability. *Eur J Control* 2020; 52: 1–10.

35. Wu Y, Wang W, Zhu H, al e. Adaptive fault-tolerant control for spacecraft formation under external disturbances with guaranteed performance. *Adv Space Res* 2023; 72: 1583–1592.

36. Jia Q, Gui Y, Wu Y, al e. Disturbance observer-based performance guaranteed fault-tolerant control for multi-spacecraft formation reconfiguration with collision avoidance. *Aero Sci Technol* 2023; 133: 108099.

37. Gao S, Liu X, Jing Y, al e. A novel finite-time prescribed performance control scheme for spacecraft attitude tracking. *Aero Sci Technol* 2021; 118: 107044.

38. Gao C, Zhang C, Liu X, al e. Event-triggering based adaptive neural tracking control for a class of pure-feedback systems with finite-time prescribed performance. *Neurocomputing* 2020; 382: 221-232.

39. Wang X, Wang X, Wang Z, al e. Composite finite-time control for PMSM with prescribed performance using disturbance compensation technique. *Control Eng Pract.* 2023; 141: 105677.

40. Li J, Xiang X, Dong D, al e. Saturated-command-deviation based finite-time adaptive control for dynamic positioning of USV with prescribed performance. *Ocean Eng* 2022; 266: 112941.

41. Zou A, Fan Z. Fixed-time attitude tracking control for rigid spacecraft without angular velocity measurements. *IEEE Trans Ind Electron* 2020; 67(8): 6795–6805.

42. Zhuang M, Tan L, Li K, al e. Fixed-time position coordinated tracking control for spacecraft formation flying with collision avoidance. *Chinese J Aeronaut* 2021; 34(11): 182–199.

43. Zheng Q, L G, ZQ G, et.al . On stability analysis of active disturbance rejection control for nonlinear timevarying plants with unknown dynamics. In: 46th IEEE Conference on Decision and Control. IEEE. ; December 12–14, 2007; New Orleans, LA, USA.

44. Wei C, Wu X, al e. Adaptive leader-following performance guaranteed formation control for multiple spacecraft with collision avoidance and connectivity assurance. *Aero Sci Technol* 2022; 120: 10726.

45. Zhang C, Ma G, Sun T, al e. Observer-based prescribed performance attitude control for flexible spacecraft with actuator saturation. *ISA Trans* 2019; 89: 84–95.

46. Wen G, Chen CP, Dou H, al e. Formation control with obstacle avoidance of second-order multi-agent systems under directed communication topology. *Sci China Inf Sci* 2019; 62: 192205.

47. Bechlioulis C, Kyriakopoulos K. Robust model-free formation control with prescribed performance for nonlinear multi-agent systems. In: Proceedings of the 2015 IEEE International Conference on Robotics and Automation. IEEE. ; May 26–30, 2015: 1268–1273.